Removal of heavy metals from water using engineered hydrochar: Kinetics and mechanistic approach

Kannan Nadarajah[1, 2, 3], Erick R. Bandala[4], Zhanying Zhang[3], Sagadevan Mundree[3], Ashantha Goonetilleke[1, 3*]

[1] School of Civil and Environmental Engineering, Queensland University of Technology, GPO Box 2344, Brisbane 4001, Queensland, Australia

[2]Department of Agricultural Engineering, Faculty of Agriculture, University of Jaffna, Sri Lanka

[3] Center for Agriculture and Bioeconomy, Institute for Future Environments, Queensland University of Technology, 2 George St, Brisbane, Queensland 4000, Australia

[4]Division of Hydrologic Sciences, Desert Research Institute, 755 E. Flamingo Road, Las Vegas, NV89119-7363, USA

[*]Corresponding author

E-mail: a.goonetilleke@qut.edu.au.

Postal address: School of Civil and Environmental Engineering, Queensland University of Technology, GPO Box 2344, Brisbane 4001, Queensland, Australia

Removal of heavy metals from water using engineered hydrochar: Kinetics and mechanistic approach

Abstract

The isotherm, kinetics, and thermodynamics parameters, and mechanisms involved in the adsorption of Pb^{2+} and Cu^{2+} ions from an aqueous solution using engineered hydrochar were investigated. The hydrochar was produced through catalytic hydrothermal carbonization of rice straw at 200°C with (engineered hydrochar) and without (hydrochar) $FeCl_3$ (1.2%) as iron catalyst which has been reported to have the ability to enhance surface properties. Batch experiments were conducted to examine the effect of sorbent dosage, pH, and initial metal ion concentration on the adsorptive performance. The results obtained revealed that the addition of iron catalyst increased the surface functional groups, and exhibit better adsorptive performance compared to non-treated hydrochar. The adsorptive performance of engineered hydrochar was higher for Pb^{2+} compared to Cu^{2+}, which can be explained by surface complexation, cationic-π interaction, and mass diffusion process with the initial removal performance limited by mass transfer process. The Langmuir isotherm model gave the best fit for the adsorption of both metals compared to the other models tested. The adsorption kinetics followed the Lagergren's pseudo-second order model. Thermodynamic parameters revealed that Pb^{2+} and Cu^{2+} adsorption by engineered hydrochar is a spontaneous and endothermic process. Moreover, this study created a new knowledge by providing an in-depth understanding of the effect of iron catalyst on the functional properties of engineered hydrochar and its adsorption mechanisms. Research on the use of catalysts in engineered hydrochar for pollutant removal is very limited. In addition, the study outcomes would contribute to the production of highly efficient magnetic hydrochars.

Keywords: Hydrochar; Heavy metals; Adsorption; Water treatment

1. Introduction

Hydrochar has attracted the interest of the scientific community because of its notable properties as an environmentally friendly, and cost-effective adsorbent for the removal of pollutants from the aqueous phase [1] [2-4]. Several different feedstock biomass have been used for hydrochar production, including a variety of agricultural wastes [5], sewage sludge [6], manure [7], and microalgae [8]. Hydrochar is produced via hydrothermal carbonisation of biomass at the temperature range of 180-240°C in the presence of hot compressed water. Hydrochar is rich in surface functional groups due to the hydrolysis and recombination reactions of biomass monomers [7]. This enhances the removal of water pollutants via adsorption. Hydrochar produced from rice straw has been reported to be highly efficient for adsorbing some organic compounds and heavy metals [6, 9-11], when oxygen-containing functional groups on its surface are increased by microwave oxidation [12], or functionalized by tailoring their physicochemical properties [9]. Some studies have suggested that the sorption capacity of hydrochar for heavy metals is lower compared to pyrolyzed biochar, because of its lower content of mineral components and oxygen-containing functional groups [13-15]. In agreement with these results, a significant amount of studies have been devoted to improve the adsorption behaviour of hydrochar with encouraging results, particularly when iron is used to modify its surface properties [16-18]. However, the production of engineered hydrochar with enhanced functional properties using catalysts still has significant knowledge gaps and requires further in-depth investigations.

Despite the wide variety of studies highlighting the significant effect on surface characteristics of hydrochar by the introduction of iron species, relatively little is known about isotherm,

kinetics, and thermodynamics parameters, or mechanisms involved in the adsorption process in the removal of heavy metals from an aqueous solution using hydrochar engineered with iron. This study focused on the use of engineered hydrochar for pollutant removal in preference to biochar and activated carbon due to the relatively high production cost of the latter products. The study assessed the potential of engineered hydrochar prepared from rice straw for the removal of Pb^{2+}, and Cu^{2+}, two heavy metals that are commonly present in aquatic environments which are discharged by industries such as metal plating and the manufacture of alloys and paints and pigments with concentrations varying widely according to the production methods used. Biosorbents are generally used to treat wastewater containing Cu^{2+} and Pb^{2+} ions in the lower concentration range of 1-100 mg/L. Furthermore, the influence of surface functional properties of hydrochar on the adsorption process, and the assessment of the detailed kinetics, isotherms, and thermodynamic parameters were undertaken to understand the adsorption mechanisms of the removal process in order to create new knowledge on hydrochar science.

2. Materials and Methods

2.1 Materials

All chemical reagents including iron chloride hexahydrate ($FeCl_3 \cdot 6H_2O$), Pb^{2+}, Cu^{2+} (primary standards), hydrochloric acid (HCl), and sodium hydroxide (NaOH) were of high purity grade obtained from Sigma Aldrich. These were used as received, without further purification.

2.2 Hydrochar production

The rice straw, which was obtained from Queensland, Australia, was sieved using an aperture size 1-2 cm to remove all inert materials, chopped into 2-7 cm pieces and milled in a biomass milling machine coupled with a 2 mm sieve (Retsch SM100, Retsch GmBH, Germany) to a particle size $\leq$ 2 mm. The homogenized biomass material was used for the HTC process. In the case of iron-modified hydrochar, the milled biomass was mixed using a 1:3 (W/V) ratio with 1.2% $FeCl_3$ solution [63]. This selection of 1:3 ratio was made based on past rsearch literature as lower solid: liquid ratio results in wastewater disposal problems [63]. The rice straw and the rice straw-iron mix was transferred to a tubular sealed reactor (GC-3 gasket closure reactor) and placed in the fluidized sand bath at 200 °C for a residence time of 3 hrs. This temperature of 200 ºC was selected based on preliminary investigations undertaken to identify the optimum temperature for hydrochar production where the biomass was subjected to different temperatures ranging from 120ºC to 280 ºC in steps of 40 ºC. The profiles of temperature and pressure were monitored every 60 min during the complete HTC process. At the end of the process, the reactor and its contents were placed in cold water to end the reactions. The contents were then processed by washing with deionized water and drying at 45ºC in a vacuum oven for characterisation.

2.3 Hydrochar characterization

2.3.1 Surface area and surface charge analyses

Surface area, pore volume and pore size distribution of the hydrochar produced was measured using Tristar II Series instrument coupled with degasser (Micrometrics, USA) from the adsorption of nitrogen at 77 K in the relative pressure range of 0.01-0.3. Samples were prepared by degassing overnight (16 hours) at 150ºC under vacuum to remove air trapped in the hydrochar. The samples were then subjected to 99 point BET surface area analysis. The BET equation was used to evaluate the adsorption process [19]. Furthermore, mesoporous volume distribution was calculated as a function of pore size based on Barrett-Joyner-Halenda (BJH) method [20]. Data collected was processed using Microactive 2 software.

The point of zero charge (pzc) analysis of the hydrochar was estimated using the pH drift method [21]. Briefly, a 0.01M NaCl solution was used and either HCl or NaOH was used to adjust the pH values between 3-11, after stabilising the suspension by gas bubbling for the removal of dissolved carbon dioxide. The hydrochar samples (0.5 g) were added to 50 mL of the prepared solutions with different pH values. The final pH values were recorded after 24 h. The initial and final pH values were used to identify pzc as the point at which values were equal.

2.3.2 Surface functional group analysis

The FTIR analysis was carried out using Alpha Fourier Transform Infrared (FTIR) spectrometer coupled with single layer diamond accessory (Madison, WI, USA). Spectra were collected within the 4,000 to 525 cm^{-1} spectral range using 64 scans at 4 cm^{-1} resolution. The background spectra was also set to correct the adsorption spectra of the samples, and it was subtracted from the FTIR spectrum. Collected FTIR spectra were interpreted using Galactic 187 Industries Corporation GRAMs32 software package (Salem, NH, USA).

2.3.3 Surface morphological analysis

The surface morphology of hydrochar samples was investigated using a Zeiss Sigma VP field emission scanning electron microscope coupled with energy dispersive X-ray analyser (FEI Company, Hillsboro, Oregon, USA). The hydrochar samples were held in a carbon tape with stainless steel stabs and were coated with a thin layer of gold under vacuum conditions (Leica Microsystems, Germany). The SE2 detector was operated at 2.5 kV and working distance of 8 mm for investigating the surface properties. The crystallographic features of the hydrochar was determined by X-ray diffraction (XRD, D8 Advance, Bucker, Germany) with a CuKal radiation source at 40 kV (Rigaku,USA), and processing current of 40 mA. Data was acquired processing the samples in the 2θ range from 3 to 60^{o} in steps of 0.01.

2.3.4 Isotherm, kinetics, thermodynamics and rate limiting factor analyses

Three different isotherm models (Langmuir, Freundlich and Temkin) were employed in order to study the nature of the adsorption (monolayer/multilayer) on the hydrochar surface and to assess the effect of surface energy on the adsorption process. For kinetics analysis, the Lagergren models (pseudo-first and pseudo-second order) were used to study the adsorption rate and the effect of equilibrium concentration on the overall removal performance of the engineered hydrochar. In addition, rate limiting analysis was performed using the Weber-Morris method [22]. Thermodynamic analysis was performed at temperatures of 30, 40, 50 and 60 ^{o} C by measuring the adsorptive performance of the engineered hydrochar. This temperature range of 30-60 ^{o}C was selected to suit the temperature of wastewater streams which are generally warmer on discharge [64]. This range of 30-60 ^{o}C has already been used by previous researchers as well [65]. The applicable equations are given in the Supplementary information.

2.3.5 Adsorption experiments

Batch adsorption experiments were conducted using 20 mL flat-bottom glass bottles where the required amount of adsorbent was added according to the experimental conditions (initial pH, adsorbent dosage, temperature, initial heavy metal concentration) in order to understand the overall adsorption mechanism for Pb^{2+} and Cu^{2+} ions (initial concentration 50 mg/L). The selection of initial concentration of 50 mg/L was based on preliminary investigations beforehand. Moreover, the initial concentration of 50 mg/ L was selected for detailed study as higher concentrations yielded lower performances as discussed in the Section, 3.2.2. The mixture was agitated at 150 rpm in an Orbital Mixer (Ratek OM, Australia). Experiments were carried out for 25 h to ensure that adsorption equilibrium was reached in the kinetics analysis.

For kinetic investigations, 0.2 mL of solution was taken out at different time intervals and for metal removal tests a volume of 1 mL was taken to minimize experimental error.
The samples were centrifuged at 10,000 rpm for 3 min to remove any remaining adsorbent and metal ion concentration was measured using ICP-OES (Varian Vista-MPX, USA). The effect of hydrochar dosage on metal ion removal was studied at 30 ºC using 50 mg/L initial heavy metal concentration at pH = 6, and hydrochar dosage ranging 1 - 15 g/L. The effect of pH on the adsorption process was assessed using 8 g/L of adsorbent dosage. The pH range tested was 2-7 and pH values higher than 7 were not selected as it can significantly influence the adsorption process due to the formation of metal hydroxide precipitates which is clearly evident from Pourbaix diagrams [66], and the initial heavy metal concentration range was 10 - 100 mg/L. Metal removal percentage and adsorption capacity were determined using Equations (1) and (2) as given below. Isotherm study was performed with initial metal concentration range of 10 - 100 mg/L with pH of 6 and adsorbent dosage of 8 g/L, whilst kinetic investigations were undertaken with initial concentrations of 30, 50 and 70 mg/L, pH of 6 and adsorbent dosage of 8 g/L.

$$Metal\ removal\ \% = \frac{C_i - C_t}{C_i} \times 100 \quad (1)$$

$$q_t = \frac{C_i - C_t}{m} \times v \quad (2)$$

Where, C_i is the initial metal concentration (mg/L), C_t is the free metal ion concentration in the solution at the sampling time (mg/L), v is the volume of metal solution (mL) and m is the mass of adsorbent (g) used. When the adsorption reached equilibrium, the free heavy metal concentration was defined as C_e and the amount of metal ion adsorbed per unit of adsorbent is q_e.

3. Results and discussion

3.1 Hydrochar characterization

3.1.1 Surface functional groups, surface area and surface charge

The FTIR analysis of the hydrochar produced with and without iron modification is shown in Fig. 1 and Fig. S1 in Supplementary information. As shown, addition of $FeCl_3$, generated significant changes particularly for the bands correlated with oxygen-containing functional groups such as carbonyl, alcoholic -OH stretching, located within the 1,240-1,670 cm^{-1} range. Moreover, detailed interpretation of the changes especially in the region 1240-1670 cm^{-1} is given in Table S1 in Supplementary information. These functional groups are considered very important for surface complexation processes [23]. The addition of iron catalyst can induce polymerization and re-arrangement reactions of monomers as well as highly active functional groups on the surface of the hydrochar, as shown in Fig. 1. The increase in electron donating sites on the surface of hydrochar would be expected to increase the removal efficiency of heavy metals [12]. The addition of the iron catalyst was also observed to enhance the intensity of the band of aromatic -C=C- and -C=O groups in the 1,584-1,685 cm^{-1} region in agreement with past studies [23]. These oxygen containing functional groups are enriched in hydrochar and are clearly visible at 1586 and 1669 cm^{-1} in the FTIR spectra given in Fig. 1.

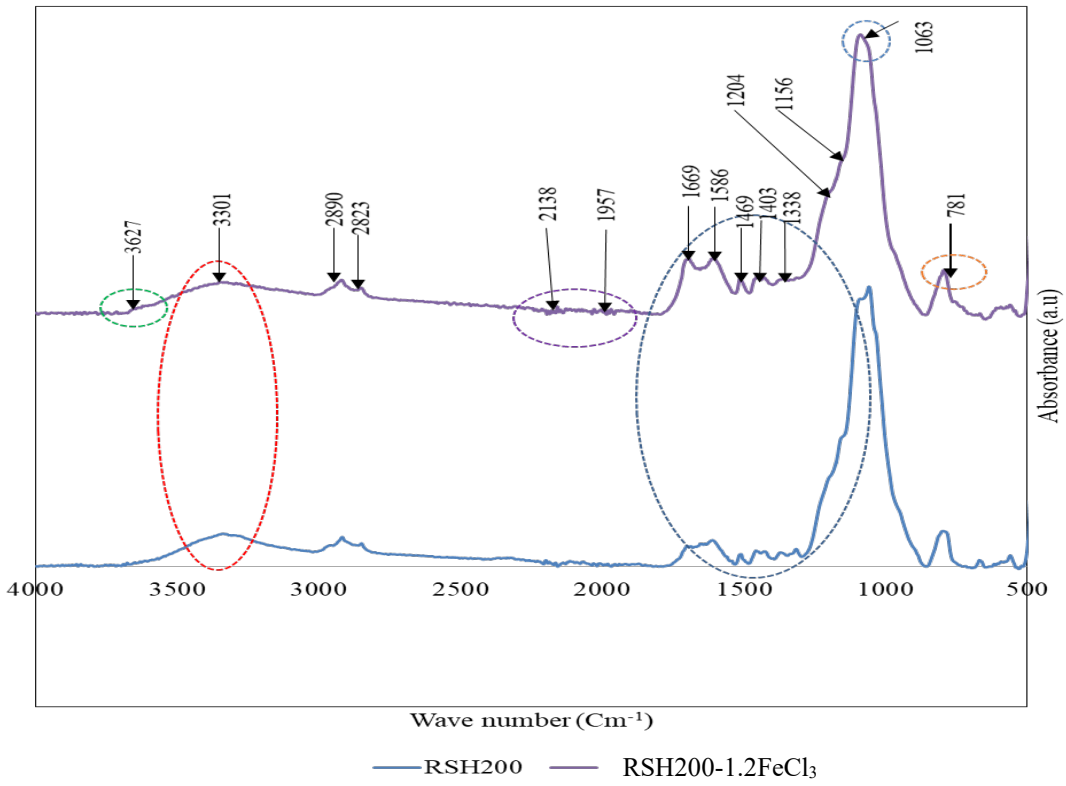

Fig. 1. FTIR analysis of catalyzed and non-catalyzed hydrochar

The bands in the region 1,302 and 1,706 cm^{-1} in Fig. 1, suggested the presence of organic residues (partially carbonised material and poly saccharrides) and carboxylic functional groups on the surface of the hydrochar due to the addition of iron catalyst together with a little increase in the surface area to 44.3 m^2/g ($RSH200\text{-}1.2FeCl_3$) compared to 39.9 m^2/g of non-catalysed hydrochar (RSH200). This increase in the surface area was due to the development of microspheres on the surface of the iron cataytic hydrochar and it was clearly observed on SEM images of the hydrochar shown in Fig.2. Moreover, it has been reported that an increase in surface area was observed in hydrochars derived from orange peel in the presence of iron catalyst. At the same time, untreated hydrochars yielded lower surface area due to incomplete carbonization and the presence of disorganized matter restraining the development of a porous structure while the deposition of iron oxide particles raised the surface area [67]. These enhanced functional groups would be expected to contribute to relatively better pollutant removal performance of hydrochar produced through iron catalytic conversion of rice straw biomass to hydrochar compared to non-catalytic hydrochar.

3.1.2 Surface morphology

The images generated from SEM analysis of the non-catalysed and the catalysed hydrochar before and after metal adsorption are shown in Fig. 2. Addition of iron catalyst was found to result in the formation of microspheres (see Fig. 2b) due to enhanced recombination reactions of biomass monomers. It is hypothesised that the microsphere formation contributed to the enhancement of the surface area described above in the case of the catalysed hydrochar, which in turn would increase its adsorptive performance. Moreover, an interesting morphological difference was noted in the hydrochar before and after adsorption of metal ions. A higher amount of deposits were observed on the hydrochar surface after the adsorption of heavy metal ions which resembles cluster layer appearance as shown in Fig. 2c. The difference in

smoothness between pristine and used material could be useful to support deposits on the surface of the hydrochar. Making the hydrochar surface rough has been reported to enhance pollutant removal performance due to the development of microspheres which can act as sites for surface functional groups. These increased surface functional groups can contribute to increased adsorptive performance of engineered hydrochar [24, 25]. The similar observation was also made in this study as shown in the Fig.2 (b).

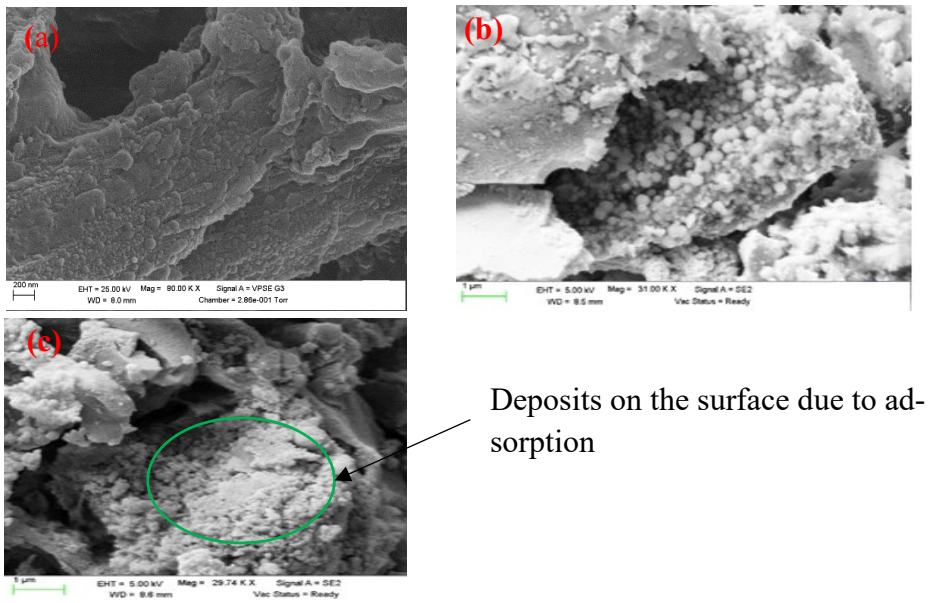

Fig. 2. SEM images of hydrochar; (a) non-catalysed: (b) before: (c) after Pb^{2+}adsorption

3.1.3 Carbon structure of hydrochar

Fig. 3 shows the XRD spectrum of catalysed and non-catalysed hydrochar, as well as the catalysed hydrochar material before and after adsorption of Pb^{2+}. The signal identified as shown in Fig. 3 at 2θ = 15.1° and 22.4° was found to correspond to the cellulose structure [3]. The signal located at 26.6° was assigned to graphite (002), while other weak signals in the diffraction pattern was related to calcite [1, 26]. From Fig. 3a, it is evident that the addition of iron catalyst reduced the cellulose content. However, it did not completely remove the cellulose from the hydrochar during the HTC process. Moreover, broadening of the XRD signal around 22.4° is due to the presence of Fe_2O_3-CHC groups [62]. As the cellulosic compound has active -OH functionalities, it is also expected will contribute to the surface complexation process for metal removal.

The XRD analysis after the adsorption of Pb^{2+} shown in Fig. 3b, indicated a change in the signals assigned to microcrystalline structure of cellulose, suggesting that this cellulosic structure was involved in the metal adsorption process as reported elsewhere [27]. The cellulosic compounds with active -OH functional groups was found to be actively participating in the surface complexation process. Therefore, the complete destruction of microcrystalline cellulose should be avoided during catalytic HTC process to retain active surface functional groups required for efficient surface complexation process.

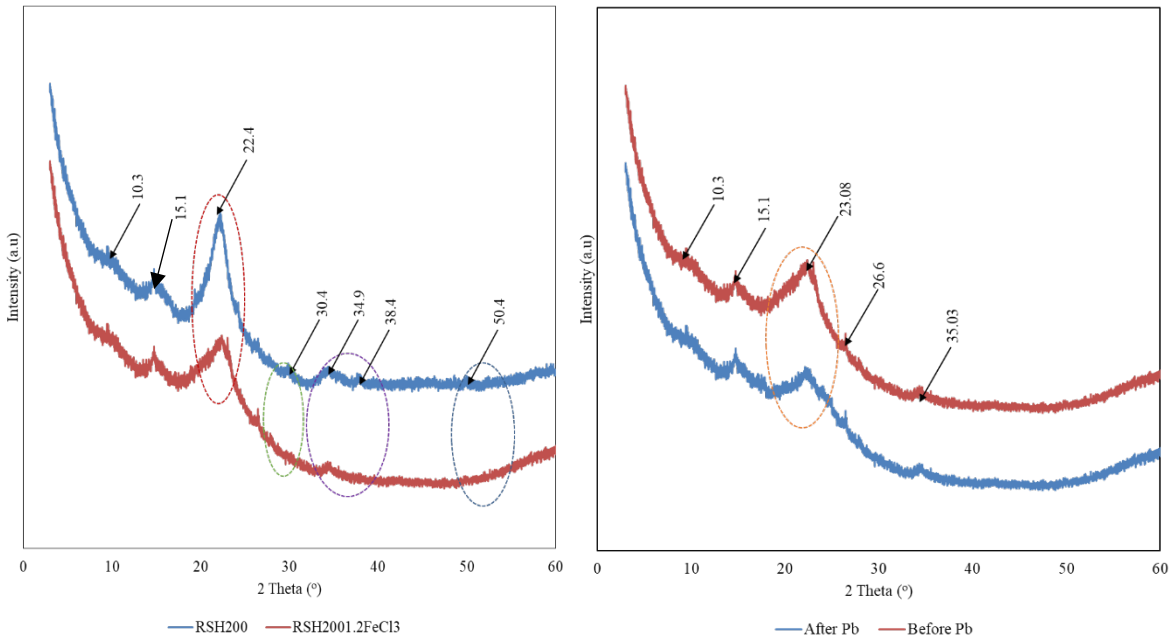

Fig. 3. (a) XRD spectrum for catalysed and non-catalysed hydrochar; and (b) catalysed hydrochar before and after Pb^{2+} adsorption

In the HTC process, cellulose decomposition of biomass feedstock has been suggested to start at temperatures over 220°C and such cellulose decomposition reaction will be complete above 260°C [3]. In this study, the HTC process was run at 200°C, allowing interaction between metal ions and the material structure. The involvement of oxygen-containing functional groups in the cellulose microcrystalline structure of hydrochar for the adsorption of Pb^{2+} was investigated by Jiang et al. [3] using XPS analysis. They found an increase in oxygen-containing groups in the hydrochar surface as the reason for the exceptional performance of biochars modified using polyethyleneimine and phosphoric acid for the adsorption of Pb^{2+} in water. Based on the FTIR analysis, in the current study, it was identified that increased oxygen-containing functional groups were responsible for the high removal rates due to the addition of iron catalyst. The -OH groups present in the cellulosic compound can also contribute to the total number of functional groups present on the surface of the hydrochar.

3.2 Heavy metals removal

The adsorptive performance of rice straw (RS), non-catalysed (RSH200) and catalysed (RSH200-1.2$FeCl_3$) hydrochar for the removal of Pb^{2+} and Cu^{2+} ions is shown in Fig. 4. The adsorptive performance of RSH200-1.2$FeCl_3$ for Pb^{2+} and Cu^{2+} ions are higher compared to RS and RSH200 because of enhanced surface functional properties of the hydrochar. The removal percentage of RS, RSH200 and RSH200-1.2$FeCl_3$ for Pb^{2+} was 54.32±1.24, 76.4±0.84 and 87.7±1.55, respectively. Moreover, the removal percentage of RS, RSH200 and RSH200-1.2$FeCl_3$ for Cu^{2+} was 33.4±0.56, 47.0±0.84 and 51.4±1.41, respectively. However, the addition of iron catalyst improved the adsorptive performance of the engineered hydrochar for Pb^{2+} ions compared to Cu^{2+}ions. This is attributed to the development of enhanced surface functional groups. The difference in adsorptive performance is attributed to the differences in ionic structure and hydration energy of Pb^{2+} and Cu^{2+} ions. Moreover, the iron catalyst has enriched hydrochar with highly reactive oxygen-containing functional groups (carbonyl, carboxylic and anhydride) required for efficient removal of metal ions because of enhanced

polymerization, condensation, and dehydration reactions of monomers derived from the hydrolysis of biomass structural compounds including cellulose, hemicellulose and lignin. The performance of engineered hydrochar was found to be relatively less effective for Cu^{2+} removal compared to non-catalysed hydrochar. This is attributed to the relatively higher hydration energy of Cu^{2+} (2,010 kJ/mol) ions compared to Pb^{2+} (1,425 kJ/mol) ions.

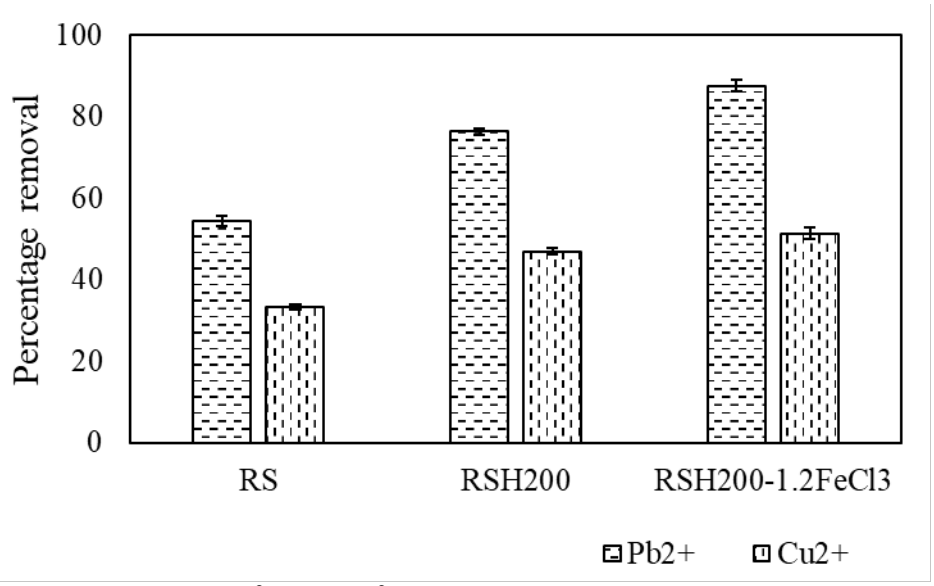

Fig. 4. Removal of Pb^{2+} and Cu^{2+} ions by RS, non-catalysed and catalysed hydrochar.

It is important to note that the initial metal ion concentration selected for this study was intended to evaluate the performance of the novel engineered hydrochar under controlled experimental conditions. From the results shown in Figure 4, it can be observed that this novel engineered hydrochar derived from rice straw biomass exhibited the potential for removal of Pb^{2+} and Cu^{2+} ions. However, future studies need to be undertaken with real wastewater containing such metal ions to derive a more detailed understanding about the removal performance of engineered hydrochar in terms of the permissible levels of metal ions. Using the best material and adsorption conditions tested, the engineered biochar produced in this study would be able to remove Pb^{2+} and Cu^{2+} ions from water samples to generate a treated effluent with metal ion concentrations below the maximum permissible level recommended by WHO (0.01 and 1.3 mg/L for Pb^{2+} and Cu^{2+}, respectively) [71] when used to treat water with initial Pb^{2+} and Cu^{2+} initial concentration as high as 1 and 2.6 mg/L, respectively, which are in the same order of magnitude usually reported in surface water samples [68,69].

3.2.1 Influence of initial pH

The influence of initial pH on Pb^{2+} and Cu^{2+} adsorption was investigated using an initial pH range between 2.0 and 7.0 as shown in Fig. 5. It is important to note that pH values higher than 7 were not selected for this analysis as it can lead to the development of metal hydroxide precipitates which significantly hinders the adsorption process. In general, it was found that heavy metal adsorption was highly dependent on initial pH and its influence was higher for Pb^{2+} compared to Cu^{2+} adsorption. For both metals, the removal capacity was found to be very low at pH = 2.0, increasing with the increase in initial pH, reaching a maximum value at initial pH = 6. This low removal performance at pH = 2 can be explained by the different pzc values of the tested hydrochar. The pzc value observed was 5.5 based on Fig. S4 in the Supplementary information, meaning that, below this value (e.g. pH = 2), the surface of the hydrochar will remain positively charged likely generating repulsion with the metal ions and impeding their

effective removal from water. As the initial pH of the mixture approaches pzc, the interaction between the surface and the ions change until pH reaches values over 5.5, where the surface charge of the hydrochar is expected to become negative, and increases the interaction with the ions.

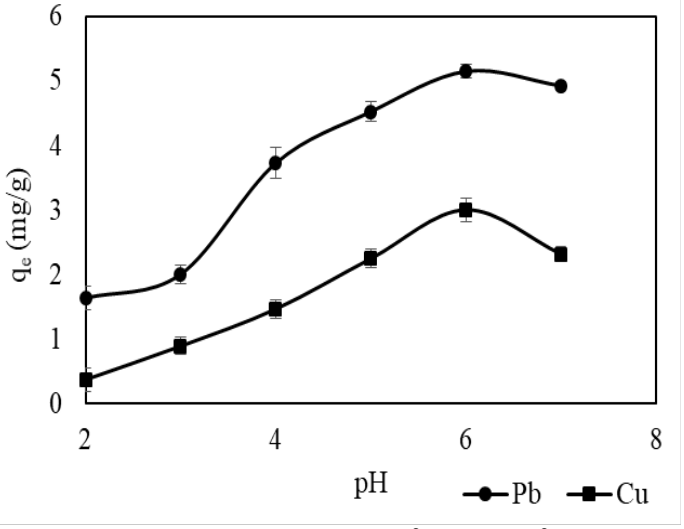

Fig. 5. Effect of initial pH on Pb^{2+} and Cu^{2+} adsorption to engineered hydrochar, RSH200-1.2$FeCl_3$ (q_e = quantity adsorbed in mg/g)

These results agree with past studies in relation to the removal of Pb^{2+} reported for chars derived from *Prosopis africana* shell via hydrothermal carbonization [28], and others where Pb^{2+} ion adsorption was found to be the highest at pH 6 in experiments conducted with activated carbon derived from apricot stone [29]. In the same way, similar results for Pb^{2+} adsorption were obtained for corn Stover hydrochar modified using polyethyleneimine or phosphoric acid, where the optimum Pb^{2+}adsorption was reported at pH = 6 [3]. At initial pH > 6, the decreasing Pb^{2+}adsorption trend is attributed to the formation of metal hydroxyl complexes of Pb^{2+} and Cu^{2+} ions [30, 31], reducing the availability of the metal ions for adsorption on the surface of the hydrochar. However, the overall trend showed a reduced capacity of the hydrochar for Cu^{2+} removal compared to Pb^{2+}, which can be explained considering hydration energy.

Hydration energy is the energy generated due to the formation of aqua-metal complexes during the dissolution of metal ions in water. The energy released by Cu dissolution is higher (2,010 kJ/mol) than by Pb (1,425 kJ/mol). Therefore, more energy is required to separate water molecules from the aqua-Cu complex in order to facilitate the surface complexation process with hydrochar. Moreover, Cu^{2+} ions will thermodynamically prefer to remain in solution rather than detaching water molecules for effective surface complexation process, resulting in lower removal efficiency. Hence, for the efficient removal of Cu^{2+} ions, the strength of the attractive forces should be further increased.

3.2.2 Effect of initial metal ion concentration

Fig. 6 shows the effect of initial Pb^{2+} and Cu^{2+} concentration on the adsorption process at 30°C. For both metal ions, adsorption efficiency increased with the increase in the initial concentration in solution. This is attributed to the high contact probability between hydrochar and the metal ions (Pb^{2+} and Cu^{2+}). The high removal capacity of hydrochar for Pb^{2+} ions over Cu^{2+} ions can be explained by chemical hardness of Pb^{2+} and Cu^{2+} ions which indicates the ability of metal ions to form strong bonds with various adsorbents [32].

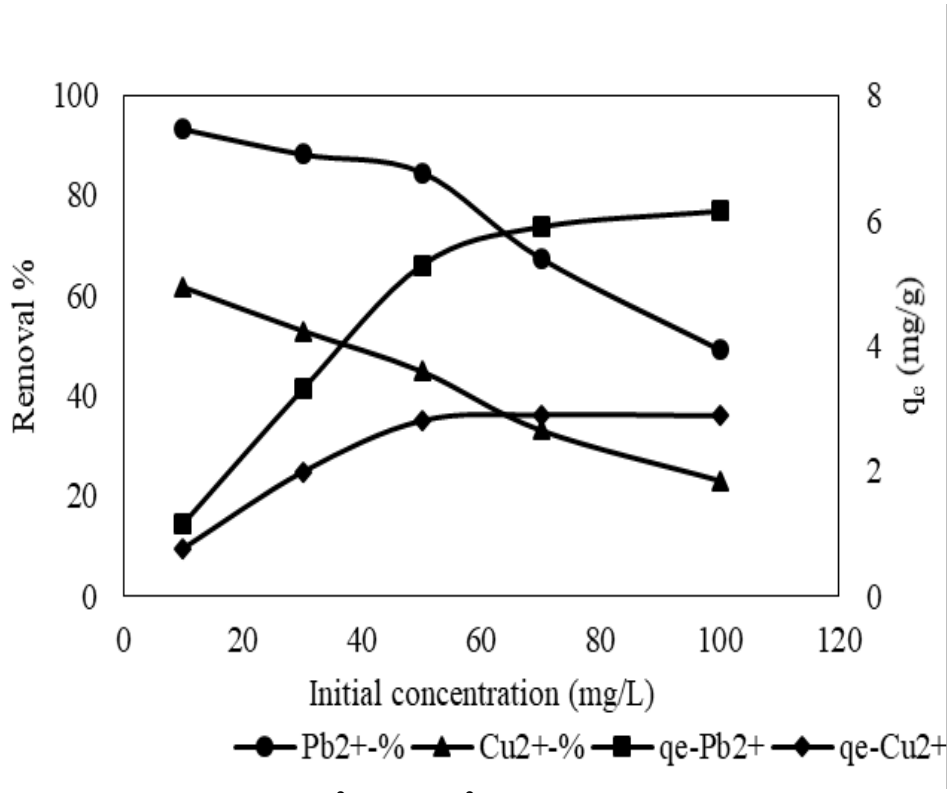

Fig. 6. Effect of initial Pb^{2+} and Cu^{2+} concentration in adsorption to engineered hydrochar, RSH200-1.2$FeCl_3$ (q_e-quantity adsorbed in mg/g)

The metal ions with high H values are able to form ionic bonds while metal ions with low H values can form covalent bonds [32]. As a result, the increase in metal ion availability in the sorption system may have less impact on the removal performance. Based on the H values of Pb^{2+} and Cu^{2+}, the trend indicated in Fig. 6 can be explained. The H value of Pb^{2+} ions (6.69) is greater than the H value of Cu^{2+} ions (2.68) [32]. Therefore, the possibility for Pb^{2+} ions to develop an association with hydrochar is higher compared to Cu^{2+} ions with increasing solution concentration. In addition, the availability of adsorption sites on hydrochar is higher at lower metal concentration because it can led to increased surface complexation. However, the adsorptive performance in terms of removal percentage for both metals drop as metal ion concentration increases because of the saturation of active functional groups present on the hydrochar surface. This is in agreement with past studies where decreasing adsorptive performance was observed in experiments conducted with hydrochar derived from *Prosopis africana* shell for the removal of Pb^{2+} and Cd^{2+} ions [28].

3.2.3 Influence of adsorbent dosage

The outcomes of the study on the effect of sorbent dosage on the removal of Pb^{2+} and Cu^{2+} ions are illustrated in Fig. 7. As shown, the adsorption capacities for both metal ions drop gradually with increasing sorbent dosage as per the definition of adsorption capacity as mg of metal ions removed per g of adsorbent. When a lower dosage is used, hydrochar exhibited excellent sorption performance for both metals, showing high absorption capacity for both Pb^{2+} and Cu^{2+} ions.

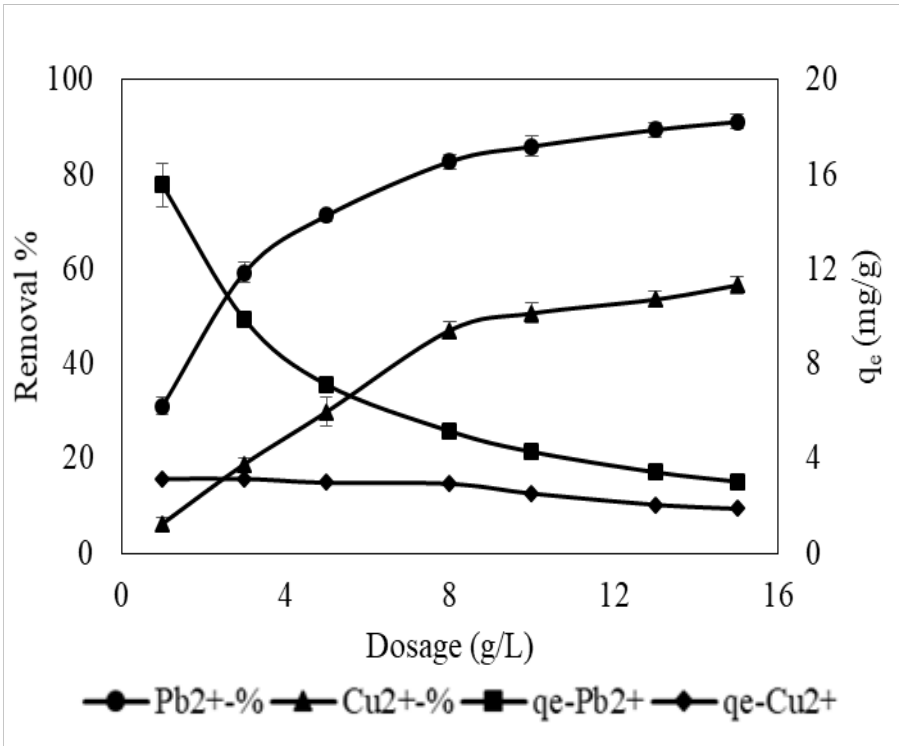

Fig. 7. Effect of adsorbent dosage on Pb^{2+} and Cu^{2+} adsorption to engineered hydrochar, RSH200-1.2$FeCl_3$ (q_e - quantity adsorbed in mg/g)

The higher mass of adsorbent available for metal ions complexation depends primarily on adsorbent dosage, facilitating the development of attractive forces for effective sorption [28]. No further change in the removal performance for both metal ions was observed for dosage values higher than 8 g/L. Moreover, the removal capacity for Pb^{2+} ions was higher than for Cu^{2+} ions with increasing sorbent dosage, in agreement with another study where similar observations were noted for Pb^{2+} removal by hydrochar derived from dehydrated banana peel prepared via hydrothermal carbonization, which was attributed to the differences in ionic characteristics between Pb^{2+} and Cu^{2+} ions [33].

Despite the fact that the number of active sites increased with increasing sorbent dosage, removal of Cu^{2+} ions was observed to be difficult compared to Pb^{2+} removal. This is attributed to the stronger ionic bonding of Cu^{2+} with water compared to Pb^{2+} ions as discussed previously [32]. Consequently, it is possible to have unused reactive sites on the surface of the hydrochar at higher adsorbent dosage when used for the removal of Cu^{2+} ions.

3.2.4 Adsorption isotherms

Three isotherm models (Langmuir, Freundlich, and Temkin) were applied to evaluate sorption capacity, adsorption intensity, and heat of sorption of the hydrochars used for the removal of Pb^{2+} and Cu^{2+} ions in aqueous solutions. The study results are given in Table 1.

Table 1. Parameters for Langmuir, Freundlich and Temkin isotherm models for Pb^{2+} and Cu^{2+} adsorption to hydrochar

Metal ion	Langmuir			Freundlich			Temkin		
	q_L	k_L	R_L^2	n	k_F	R_F^2	A_T	B_T	R_T^2
Pb^{2+}	6.75	0.31	**0.997**	2.50	1.30	0.860	4.39	1.19	0.930
Cu^{2+}	4.0	0.06	**0.994**	2.19	0.74	0.877	0.91	0.75	0.917

As shown in Table 1 and Fig.S5, the Langmuir model gave the best fit (R_L^2 of Pb^{2+}= 0.997; R_L^2 of Cu^{2+} = 0.994) for both metal ions compared to Freundlich and Temkin models. Therefore, the Langmuir model parameters were taken into account for developing insights into the adsorption mechanism of engineered hydrochar for Pb^{2+} and Cu^{2+} ions. The Langmuir model parameters, q_L, k_L and R_L^2 represent equilibrium adsorption capacity (mg/L), Langmuir constant related to energy of sorption (L/mg) and regression coefficient, respectively. Moreover, outcomes of the Langmuir analysis can be applied to study the nature of the deposition of metal ions on the surface of the engineered hydrochar.

The Langmuir constant (k_L) was estimated as 0.3 and 0.06 L/mg for Pb^{2+} and Cu^{2+}, respectively, suggesting that the bonding energy for Pb^{2+} adsorption to hydrochar is greater than the bonding energy for Cu^{2+} ions. The results also suggest the association of Pb^{2+}ions with hydrochar is stronger compared to Cu^{2+} ions, which supports the results of better removal performance for Pb^{2+} ions [34]. The better fit of the Langmuir model also indicated monolayer adsorption of the two metal ions to hydrochar and it is in agreement with other studies reporting the adsorption of Pb^{2+} to biochar from fresh and dehydrated banana peel [33] and pomegranate peel [35]. Moreover, this monolayer adsorption is significant as it develops strong association between the surface of the hydrochar and metal ions to provide better adsorptive performance.

3.2.5 Adsorption kinetics

The results obtained after applying pseudo-first and pseudo-second order kinetics for fitting of the experimental results on Pb^{2+} and Cu^{2+} adsorption to hydrochar are shown in Table 2. As shown, the pseudo-second order kinetic model was found with the best correlation coefficient values. Moreover, in pseudo-second order analysis, the influence of equilibrium concentration has been eliminated to obtain a better understanding of the adsorption mechanism. As chemisorption process occurs during adsorption of metal ions, it takes a relatively longer time to reach equilibrium and will generate poor fit for the kinetic analysis.

The q_{e2}, R_2^2, and k_2 values were used for the interpretation of kinetic analysis outcomes as shown in Table 2. Fig. S2 and S3 in Supplementary information show the outcomes of the pseudo second order kinetics obtained for Pb^{2+} and Cu^{2+} ions. As indicated in Table 2, the R_2^2 values obtained from Fig. S2 and Fig. S3 using linear regression for both metal ions at different initial concentrations are near to 1.0, which indicates that the removal rate is influenced by the equilibrium concentration, and there is involvement of the chemisorption process during adsorption.

Moreover, q_{e2} values obtained for Cu^{2+} and Pb^{2+} ions are comparable with experimental values using different initial concentrations as indicated in Table 2. Furthermore, the q_{e2} values obtained for the pseudo-second order kinetics are comparable with previous studies. For example, Singh et al.[36] used a low-cost char synthesized from waste polyvinyl chloride, polyethylene terephthalate, and polyethylene for adsorbing arsenic. They also found the pseudo-second order kinetics model gave the best fit for the experimental results and obtained

q_{e2} values in the range 1.8-1.9 mg/g and k_2 values in the range 1-1.4 min^{-1}, depending on the char type, which is in the same order of magnitude reported here. In another study, Liu et al. [10] used corn straw and corncob biomass to generate hydrochar and tested for Cd^{2+} and Cr(VI) adsorption. Liu et al. [10] suggested that the good performance of the hydrochars tested for the removal of Cr(VI) was probably related to the number of oxygenated functional groups on the surface of the hydrochar.

Table 2. Parameters of pseudo-first and pseudo-second order kinetics models for Pb^{2+} and Cu^{2+} adsorption to customized hydrochar

Ion	C_i, mg/L	pseudo-first order			pseudo-second order		
		q_{e1}, mg/g	k_1, min^{-1}	R_1^2	q_{e2}, mg/g	k_2, g/mg min	R_2^2
Pb^{2+}	30	1.2	0.001	0.81	3.60	0.005	**0.99**
	50	1.5	0.002	0.67	5.70	0.003	**0.99**
	70	1.1	0.002	0.60	6.25	0.005	**0.99**
Cu^{2+}	30	0.9	0.002	0.76	2.32	0.014	**0.99**
	50	1.1	0.002	0.75	3.30	0.008	**0.99**
	70	1.1	0.002	0.80	3.41	0.008	**1.00**

Moreover, the high content of oxygenated functional groups on the surface of the hydrochar investigated in this study could be also be the cause of the similar results achieved and mechanisms identified for Pb^{2+} and Cu^{2+} removal. However, more detailed investigations are needed to confirm this hypothesis.

3.2.6 Adsorption thermodynamics

The study on adsorption thermodynamics of the engineered hydrochar was beneficial to investigate the effect of adsorption temperature on the removal performance and to study whether the adsorption is endothermic or spontaneous in nature. Thermodynamic parameters such as Gibbs free energy (ΔG^o), change in enthalpy (ΔH^o) and entropy (ΔS^o) for Pb^{2+} and Cu^{2+} adsorption was analysed and are shown in Table 3. The value of ΔG^o was estimated because it is important to study the spontaneous nature and type of adsorption process involved in the removal of Pb^{2+} and Cu^{2+} ions [37]. Furthermore, this parameter is also used to distinguish physisorption and chemisorption processes responsible for the surface complexation process [38].

The negative value of ΔG^o for both metals at all levels of temperature indicates the spontaneous nature of adsorption of Pb^{2+} and Cu^{2+} ions to the surface of the hydrochar. The higher negative ΔG^o of Pb^{2+} ions suggest greater spontaneity compared to Cu^{2+} ions during the adsorption process [38]. Furthermore, the positive value of ΔH^o observed suggest that the adsorption was an endothermic process, meaning that the removal efficiency of the two metals can be increased by increasing the temperature of the system up to a limit [39]. These effects were confirmed by the experimental values obtained for both metal ions. As ΔG^o values obtained for both metals was less than -40 kJ/mol, there is the possibility of the involvement of physisorption process after the formation of surface monolayer on the hydrochar surface. The positive value of ΔS^o in Table 3 suggests that the affinity of hydrochar for both metal ions was strong and the adsorption of these metal ions to the surface of the hydrochar may lead to some structural changes [40]. Moreover, the higher positive value of ΔS^o for Pb^{2+} ions compared to Cu^{2+} ions suggests stronger association of Pb^{2+} ions with the surface of the hydrochar. Furthermore,

positive value of ΔS^o also reflects increasing randomness at the solid/ liquid interface during the sorption of both metal ions to the surface of the hydrochar [40]. This increasing randomness is higher for Pb^{2+} ions compared to Cu^{2+} ions due to higher ΔS^o value for Pb^{2+} adsorption. These values are in conformity with reported past research results on the thermodynamics of heavy metal adsorption [28].

Table 3. Thermodynamic parameters of Pb^{2+} and Cu^{2+} adsorption to customized hydrochar

Metal ion	Temperature, K	Thermodynamic parameters		
		ΔG^o, kJ/mol	ΔH^o, kJ/mol	ΔS^o, J/mol K
Pb^{2+}	303	-29.16	15.13	46.71
	313	-29.63		
	323	-30.10		
	333	-30.50		
Cu^{2+}	303	-14.56	10.18	14.45
	313	-14.70		
	323	-14.80		
	333	-14.90		

3.2.7 Rate limiting factor analysis

The movement of heavy metal ions to the surface and into the pore spaces of hydrochar is influenced by the rate limiting effect. Therefore, the analysis of the rate limiting effect is important to identify the most significant rate limiting process during the adsorption of Pb^{2+} and Cu^{2+} ions. The kinetics model described by Weber-Morris graphical method was used to undertake the rate limiting factor analysis for Pb^{2+} and Cu^{2+} ions, which assumes that, if the rate limiting step of the process is intraparticle diffusion, a plot of solute sorbent against square root of contact time should yield a straight line passing through the origin [41]. The Weber-Morris parameters, namely, adsorption capacity (q_t, mg/g), intraparticle diffusion rate constant (K_{wm}, mg/g.min$^{1/2}$), and the intercept (I, mg/g) estimated for Pb^{2+} and Cu^{2+} analysis are shown in Fig. 8. The values for K_{wm} and I were obtained from the slope and intercept for three different concentrations as shown in Fig. 8.

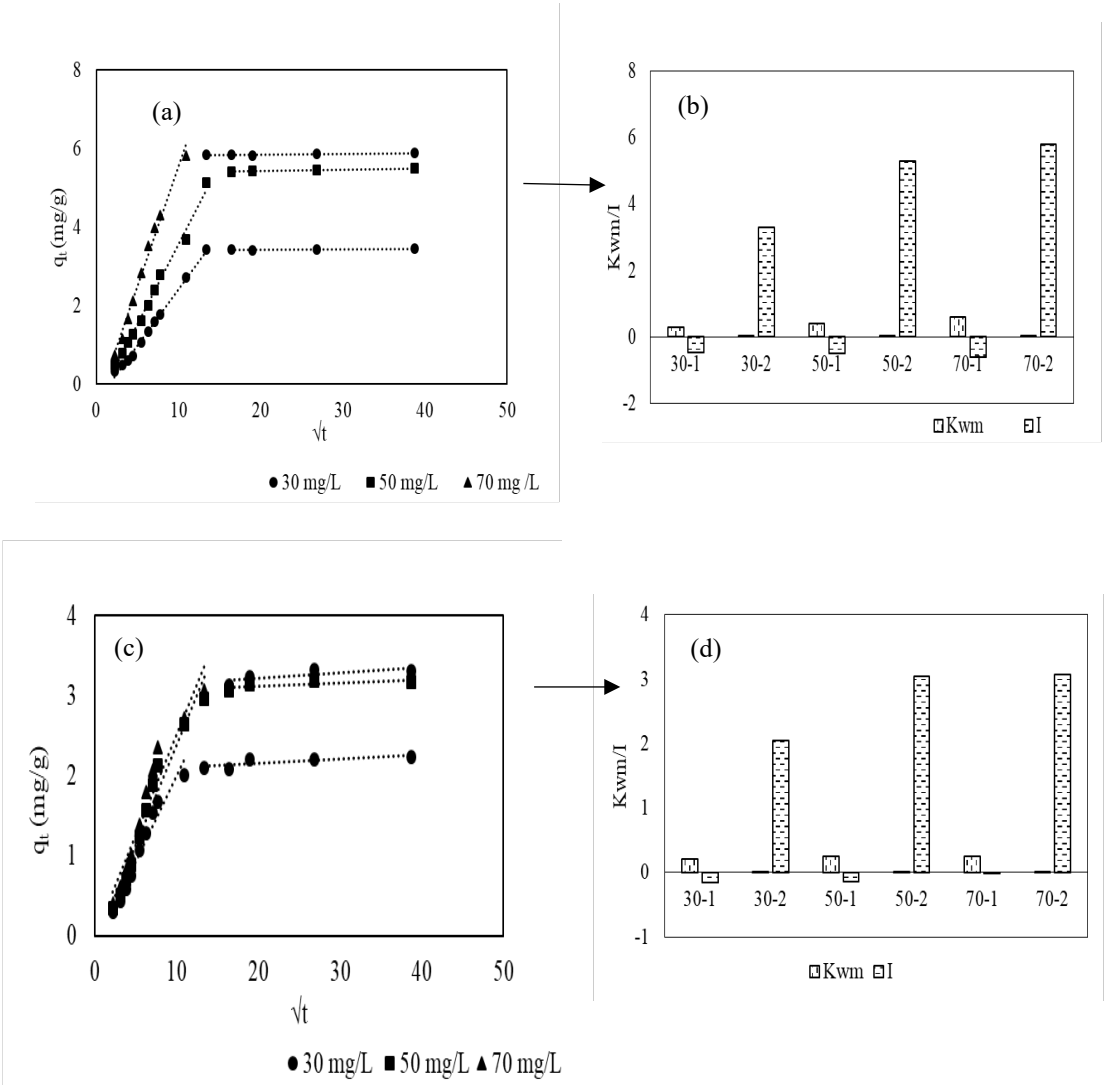

Fig. 8. Rate limiting factor analysis of Pb^{2+} (a and b) and Cu^{2+} (c and d) adsorption by hydrochar

As shown in Fig. 8, both metal ions (Pb^{2+} and Cu^{2+}) produced a similar pattern at different initial concentrations in the Weber-Morris analysis. The relationship between q_t and $t^{1/2}$ was not linear over the whole time period considered. Furthermore, the linearity test was performed separately for the different scenarios as indicated in Fig. 8. Two distinctly different phases were evident from the Weber- Morris analysis for Pb^{2+} and Cu^{2+} ions. The first linear portion of the q_t versus $t^{1/2}$ plot represents metal ions mass movement from the solution to the surface of the hydrochar and the second linear portion is associated with the movement of metal ions into the surface and internal openings of the hydrochar. Furthermore, the higher slope for the first portion suggested the rapid movement of metal ions from the solution to the surface of the hydrochar due to attractive forces developed by surface functionalities of the hydrochar [41].

The lower slopes of the second linear portion of the Weber-Morris analysis show the effect of intraparticle diffusion rate after a long reaction time. As evident from the analysis of K_{wm} (Fig. 8b and 8d), the influence of the boundary layer is stronger in the second phase of adsorption for both metal ions, resulting in low K_{wm} values. When more molecules were available in the system, intraparticle diffusion rate was also higher. However, it reduced significantly as the thickness of the boundary layer increased. It has been suggested that the intraparticle diffusion

rate could be increased by breaking the boundary layer, but this is only possible when enough internal openings are available in the hydrochar to accommodate metal ions [41]. It has been further reported that intercept value I > 1.0 suggests that the rate limiting effect is controlled by both, boundary layer thickness and intraparticle diffusion rate [42]. Therefore, values obtained for I from the second phase of adsorption of both metal ions at different concentrations suggest the influence of both, boundary layer and intraparticle diffusion on the overall removal performance.

3.2.8 Adsorption mechanism

An understanding of the adsorption mechanism of engineered hydrochar for Pb^{2+} and Cu^{2+} ions is very important for enhanced custom design of the surface properties of engineered hydrochar. Among the different adsorption mechanisms, surface complexation is a dominant process that is actively involved in metal removal by hydrochar. Accordingly, the surface complexation process was evaluated using the changes in FTIR spectra after the adsorption of Cu^{2+} and Pb^{2+} ions. Addition of iron catalyst has the ability to enhance oxygen containing functional groups on the surface of the hydrochar due to enhanced polymerization and recombination reactions of monomers. FTIR analysis was also performed before and after adsorption in order to study the involvement of surface functionalities in the removal of heavy metal ions from water. The changes in the FTIR spectra due to adsorption of Pb^{2+} and Cu^{2+} ions are shown in Fig. 9. This clearly indicates the involvement of oxygen-containing functional groups, anhydride groups and -C=C- groups in the removal process of Pb^{2+} and Cu^{2+} ions.

Wang et al. [12] suggested that Pb^{2+} removal is related with the increase in coverage of surface hydroxyl groups in chars modified with mineral oxides, which was also found to decrease the pH at the point of zero charge. In the past, comparatively better Pb^{2+} removal due to increased O-containing functional groups for chars modified with iron, particularly biochars, has been reported [43, 44]. The signal at 1,678, 1,609, and 1,620 cm^{-1} attributed to C=C was also identified as prominent in the removal of heavy metal ions from aqueous solution and changes in band intensities responsible for C=C have been observed to be related to the adsorption of Cu^{2+} and Pb^{2+} ions [45]. These observations are in conformity with the observations made in this study in terms of the development of oxygen containing groups and their involvement in the metal removal process.

The interaction of the metals with the different functional groups on the surface of the hydrochar can be observed as band intensities at 1,462 (aromatic C=H stretching), 3,316 (free and H bonded -OH groups), 1,080 (-RO stretch) and 781 cm^{-1} (aromatic -CH_3) changed after the adsorption of metal ions Pb^{2+} and Cu^{2+} as indicated in the Fig. 9. The effect seems to be more prominent for Pb^{2+} ions compared to Cu^{2+}, which is attributed to the higher affinity of the formers with ketone, ether, and hydroxyl groups while Cu^{2+} has been suggested to have higher preference for acidic functional groups [33]. Band intensities for strong surface functionalities, 1,830 cm^{-1} (anhydride -C=O), 1,773 cm^{-1} (conjugated anhydride -CO), and 1,430 cm^{-1} (acid -OH bending) also changed after metal ion adsorption. The interaction of metal ions with the strong surface oxygen-containing functionalities (carbonyl, carboxylic and anhydride) caused changes in band intensities as shown in Fig. 9, suggesting surface complexation being one of the mechanisms involved in the adsorption process, in agreement with past studies [46].

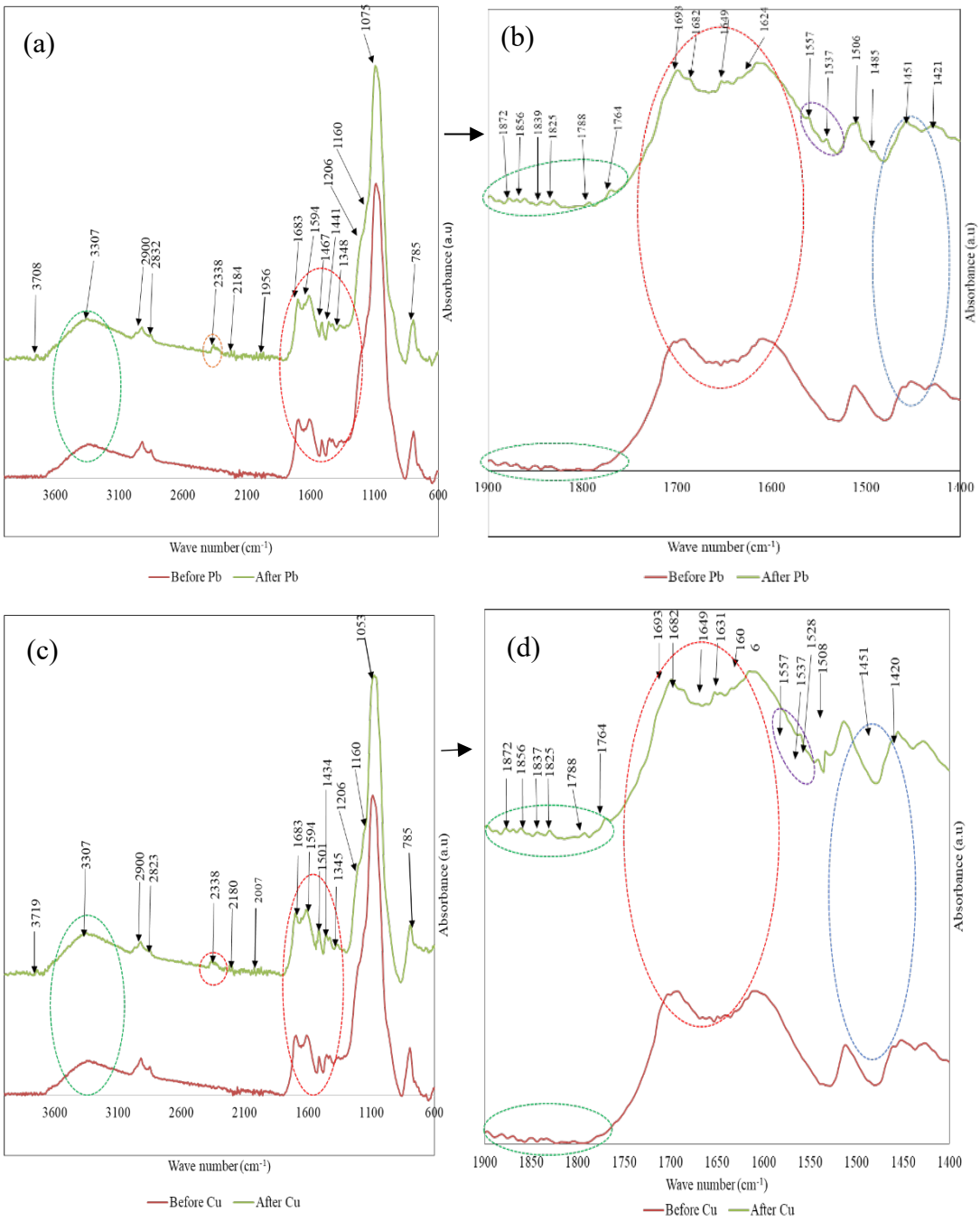

Fig. 9. FTIR analysis for Pb^{2+} (a and b) and Cu^{2+} (c and d) adsorption

The observed changes in the band intensities of aromatic -C=C suggest that heavy metal ion-π interaction can be another sorption mechanism which is also involved in the removal process. Carbon-carbon double bonds are rich in π-electrons which interact with metal ions to generate strong interactions generally involving d-orbitals in metal ions and π-electrons of aromatic rings in unsaturated aromatic systems of the heterocyclic region of hydrochar [12, 46]. Similar observations have been made by past researchers who have used these changes as evidence to explain the involvement of different surface functional groups in the removal of heavy metal ions by various adsorbents [47-49].

The peaks represent aromatic -C=O and C=C functional groups which occur at 1,404 cm^{-1} before and 1,412 cm^{-1} after adsorption [48]. The bands at 1,172 cm^{-1} and 1,157 cm^{-1} correspond to -CO stretching in alcohols and phenols before and after adsorption, respectively [46]. Strong peaks at 983 cm^{-1} and 985 cm^{-1} are assigned to aromatic rings in biochar before and after adsorption, respectively [50]. Therefore, it can be concluded that carbonyl, anhydride, hydroxyl, alkane and alkene (aromatic and aliphatic) groups participate in the adsorption of heavy metals. This observation reflects the complex nature of the association between metal ions and surface functionalities of hydrochar. Hence, the enrichment of such functional groups can increase the adsorptive performance of engineered hydrochar.

In addition to functional groups, the surface area of non-catalysed and optimized hydrochar was 39.9 and 44.3 m^2/g, respectively. However, the increase in surface area is not significant due to the addition of iron catalyst. Hence, the development of surface functional groups is the key factor that contributed to the enhanced removal performance of the catalysed hydrochar. Jain et al. [51] have collated information about the BET surface area of hydrochars obtained from different feedstock materials, methods and catalyst employed. They reported values ranging from 0.2 to 673 m^2/g for hydrochar obtained from orange peel and glucose, respectively.

The BET surface area of the material obtained in this study is comparable with those reported for hydrochar using pine cone and citric acid as catalyst (BET = 34 m^2/g [52]), walnut shells (BET = 31 m^2/g [53]), and hazelnut shells (BET = 45 m^2/g [54]). The pzc of the obtained materials was 5.5, which is also comparable with other studies. For example, Huangfu et al. [55] reported a pzc value of 5.8 for hydrochar produced from rice hull at low temperature (<100° C) and atmospheric pressure. In agreement with these results, it is expected that the engineered hydrochar used in this study will remain positively charged below the identified pzc value and became negatively charged as the pH of the suspension increases above 5.5 [56]. However, for the efficient removal of Pb^{2+} and Cu^{2+} ions, the surface of the hydrochar should be kept negative so as to attract positively charged metal ions effectively. Hence, keeping the pH value above 5.5 is ideal to keep the surface of the hydrochar negative. Research literature has reported that biochar surface is negatively charged as pH of the medium is greater than pzc [60]. However, for this study engineered hydrochar was used rather than biochar due to low production costs [51].

Based on isotherm, kinetic and thermodynamic analyses, a simplified model was developed to suggest key mechanistic processes involved in the removal of heavy metal ions by the hydrochar used in this study. The microspheres observed on the surface of the hydrochar are considered to provide an effective surface area and active sites for the interaction of reactive functional groups with metal ions in the adsorption process as shown in Fig. 10. Hydrochar materials generally include hydrophobic sites, partially carbonized portion, carbonized portion, pore spaces and organized aromatic rings (Loblolly) which act as functional pockets and exert significant influence on the removal of pollutants from aqueous solutions.

Non-carbonized portion and hydrophobic sites of hydrochar have been suggested as the main structures responsible for the removal of pollutants by adsorption [51]. The major processes contributing to the removal of metal ions are suggested to include surface complexation and metal ion- π interaction, the former is considered mainly due to the reactive surface functional groups present on the surf ace of the hydrochar [57]. Different oxygen containing functional groups have been identified on the surface of the hydrochar as discussed previously. Among these, some functional groups are stronger. For example, carbonyl and carboxylic functional

groups are generally classified as having the ability to strongly associate with heavy metal ions present in solution [58].

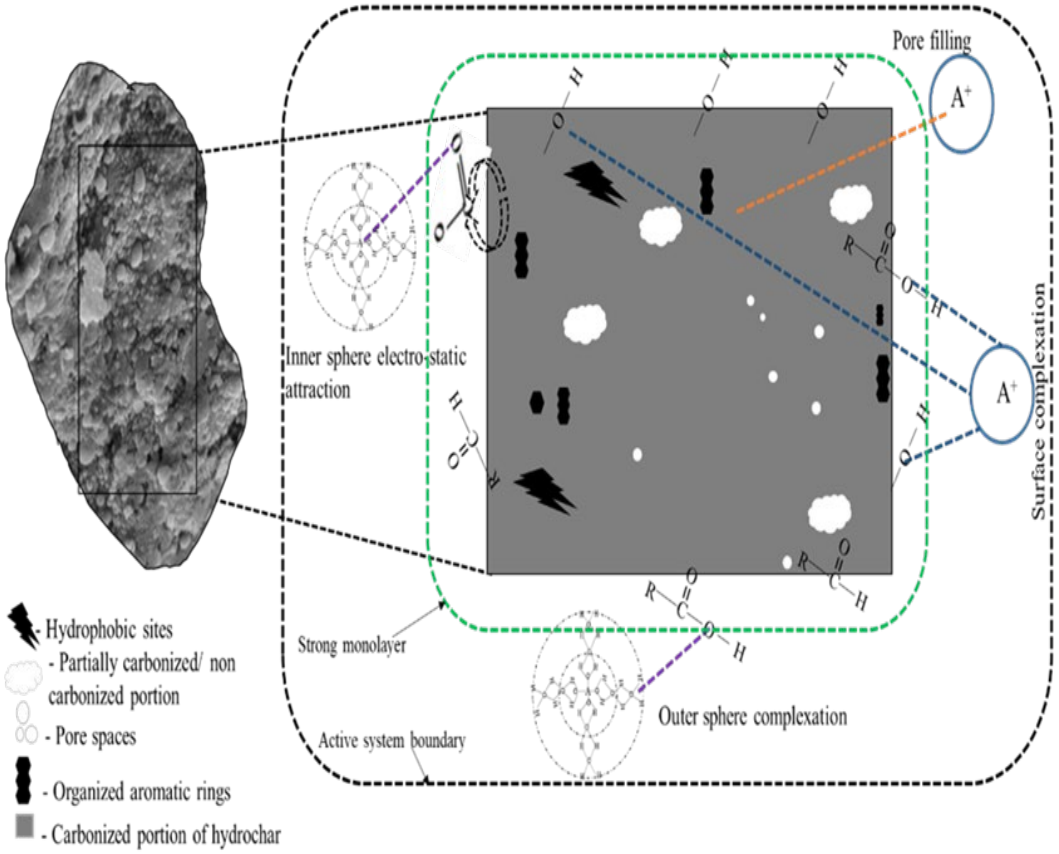

Fig. 10. Model for explaining heavy metal adsorption to hydrochar

However, the ability of the two metal ions studied to generate stronger inner sphere and outer sphere metal-aqua complexes with water was also found to play a significant role in the removal process. The relatively higher capability of Cu^{2+} ions to generate outer sphere metal-aqua complexes may be considered as a rational way to explain why its removal is more difficult compared with Pb^{2+} ions. Surface complexation can be related to both, strong attractive forces contributing to generate a monolayer on the surface of the hydrochar and weak attractive forces responsible for forming sorbate-sorbent network once the monolayer has been created.

Generally, strong attractive forces are involved in the chemisorption process, while weak attractive forces are involved in the physisorption process [59]. Participation of the strong oxygen functional groups in the monolayer formation on the hydrochar surface is evidenced by the isotherm models and FTIR analysis as discussed above and these functional groups are hydrophilic in nature. This hydrophilicity can significantly contribute to the overall metal removal performance [60, 61]. The ionic layers formed over the initial monolayer is expected to participate in the physisorption process which is weak and liable to be dissociated, which is in line with the results from FTIR analysis and in agreement with past studies [46].

4 Conclusions

Based on the results obtained from this study, it can be concluded that the adsorptive performance of the engineered hydrochar for Pb^{2+} and Cu^{2+} ions improved significantly compared to raw biomass due to the enhanced surface properties, surface functional groups

and constricted carbon structure. The results of the XRD, SEM and FTIR analyses of the engineered hydrochar before and after the adsorption of Pb^{2+} ions showed the involvement of microcrystalline cellulose in metal binding process, developments of surface deposits due to metal ion deposition and the involvement of highly reactive surface functional groups, namely, hydrophilic (carbonyl, carboxylic and anhydride) and hydrophobic (aromatic) groups in the surface complexation process of metal ions. It is evident from the in-depth investigation that for the enhanced adsorptive performance, surface functional groups (carbonyl and carboxylic) and surface microspheres need to be developed on the surface of the engineered hydrochar for the removal of Pb^{2+} and Cu^{2+} irons from aqueous phase together with optimum adsorption parameters obtained in this study, adsorbent dosage of 8 g/L, pH of 6 and initial metal concentration of 50 mg/L.

These results are very important in the study of the metal binding mechanism of engineered hydrochar during adsorption. Moreover, the sorption isotherms of Pb^{2+} and Cu^{2+} ions were well described by the Langmuir model, while kinetics of Pb^{2+} and Cu^{2+} removal followed the pseudo second order model. The thermodynamic studies revealed that the adsorption of Pb^{2+} and Cu^{2+} ions on engineered hydrochar is a spontaneous and endothermic process. Therefore, the study results suggest that the catalytic production of engineered hydrochar from rice straw biomass can be an efficient way to convert waste rice straw biomass into an efficient low-cost hydrochar for the removal of metal ions from wastewater. Considering the optimum adsorption conditions identified in this study, the best material identified would be capable of reducing the concentration of both, Pb^{2+} and Cu^{2+} ions below, for example, the maximum discharge limits stablished by the U.S. Environmental Protection Agency (1.0 mg/L in both cases) [70] for wastewater effluent with initial concentration of Pb^{2+} and Cu^{2+} as high as 8 mg/L. However, further modification of this hydrochar is required to improve its adsorptive capacity to suit industrial applications.

Acknowledgements
The authors would like to acknowledge Queensland University of Technology (QUT) for providing the postgraduate research scholarship for the first author to undertake this study. We would also like to thank the Central Analytical Research Facility (CARF) operated by the Institute of Future Environments (QUT) where the data reported in this paper were obtained. Access to CARF is supported by generous funding from the Science and Engineering Faculty (QUT). These organisations did not participate in the study design; in the collection, analysis and interpretation of data; in the writing of the manuscript; and in the decision to submit the article for publication.

References

[1] Chen, X.q., B. Li, Y. Shen, and J.-Z. Guo, *Facile synthesis of calcite-impregnated hydrochar with high sorption capacity for Cu (II) from aqueous solution.* ACS omega, 2019. **4**(12): p. 15022-15029.

[2] Chen, H., Y. Zhou, H. Zhao, and Q. Li, *A comparative study on behavior of heavy metals in pyrochar and hydrochar from sewage sludge.* Energy Sources, Part A: Recovery, Utilization, and Environmental Effects, 2018. **40**(5): p. 565-571.

[3] Jiang, Q., W. Xie, S. Han, Y. Wang, and Y. Zhang, *Enhanced adsorption of Pb (II) onto modified hydrochar by polyethyleneimine or H3PO4: An analysis of surface property and interface mechanism.* Colloids and Surfaces A: Physicochemical and Engineering Aspects, 2019. **583**: p. 123962.

[4] Li, B., J.-Q. Lv, J.-Z. Guo, S.-Y. Fu, M. Guo, and P. Yang, *The polyaminocarboxylated modified hydrochar for efficient capturing methylene blue and Cu (II) from water.* Bioresource technology, 2019. **275**: p. 360-367.

[5] Khushk, S., L. Zhang, A.M. Pirzada, M. Irfan, and A. Li. *Cr (VI) heavy metal adsorption from aqueous solution by KOH treated hydrochar derived from agricultural wastes*. 2019. AIP Publishing LLC.

[6] Zhang, H., X. Yue, F. Li, R. Xiao, Y. Zhang, and D. Gu, *Preparation of rice straw-derived biochar for efficient cadmium removal by modification of oxygen-containing functional groups.* Science of the Total Environment, 2018. **631**: p. 795-802.

[7] Gascó, G., J. Paz-Ferreiro, M.L. Álvarez, A. Saa, and A. Méndez, *Biochars and hydrochars prepared by pyrolysis and hydrothermal carbonisation of pig manure.* Waste management, 2018. **79**: p. 395-403.

[8] Saber, M., F. Takahashi, and K. Yoshikawa, *Characterization and application of microalgae hydrochar as a low-cost adsorbent for Cu (II) ion removal from aqueous solutions.* Environmental Science and Pollution Research, 2018. **25**(32): p. 32721-32734.

[9] Peng, X., Z. Yan, X. Cheng, Y. Li, A. Wang, and L. Chen, *Quaternary ammonium-functionalized rice straw hydrochar as efficient adsorbents for methyl orange removal from aqueous solution.* Clean Technologies and Environmental Policy, 2019. **21**(6): p. 1269-1279.

[10] Li, Y., N. Tsend, T. Li, H. Liu, R. Yang, X. Gai, H. Wang, and S. Shan, *Microwave assisted hydrothermal preparation of rice straw hydrochars for adsorption of organics and heavy metals.* Bioresource technology, 2019. **273**: p. 136-143.

[11] Abaide, E.R., G.L. Dotto, M.V. Tres, G.L. Zabot, and M.A. Mazutti, *Adsorption of 2–nitrophenol using rice straw and rice husks hydrolyzed by subcritical water.* Bioresource technology, 2019. **284**: p. 25-35.

[12] Wang, L., Y. Wang, F. Ma, V. Tankpa, S. Bai, X. Guo, and X. Wang, *Mechanisms and reutilization of modified biochar used for removal of heavy metals from wastewater: a review.* Science of the total environment, 2019. **668**: p. 1298-1309.

[13] Inyang, M., B. Gao, Y. Yao, Y. Xue, A.R. Zimmerman, P. Pullammanappallil, and X. Cao, *Removal of heavy metals from aqueous solution by biochars derived from anaerobically digested biomass.* Bioresource technology, 2012. **110**: p. 50-56.

[14] Demirbas, A., *Heavy metal adsorption onto agro-based waste materials: a review.* Journal of hazardous materials, 2008. **157**(2-3): p. 220-229.

[15] Xu, X., Y. Zhao, J. Sima, L. Zhao, O. Mašek, and X. Cao, *Indispensable role of biochar-inherent mineral constituents in its environmental applications: a review.* Bioresource Technology, 2017. **241**: p. 887-899.

[16] Çatlıoğlu, F.N., S. Akay, B. Gözmen, E. Turunc, I. Anastopoulos, B. Kayan, and D. Kalderis, *Fe-modified hydrochar from orange peel as adsorbent of food colorant Brilliant Black: process optimization and kinetic studies.* International Journal of Environmental Science and Technology, 2020. **17**(4): p. 1975-1990.

[17] Teng, F., Y. Zhang, D. Wang, M. Shen, and D. Hu, *Iron-modified rice husk hydrochar and its immobilization effect for Pb and Sb in contaminated soil.* Journal of Hazardous Materials, 2020: p. 122977.

[18] Feng, Y., P. Liu, Y. Wang, Y.Z. Finfrock, X. Xie, C. Su, N. Liu, Y. Yang, and Y. Xu, *Distribution and speciation of iron in Fe-modified biochars and its application in removal of As (V), As (III), Cr (VI), and Hg (II): An X-ray absorption study.* Journal of hazardous materials, 2020. **384**: p. 121342.

[19] Zhang, C. and N. Lu, *Augmented Brunauer–Emmett–Teller equation for water adsorption on soils.* Vadose Zone Journal, 2019. **18**(1): p. 1-12.
[20] Bardestani, R., G.S. Patience, and S. Kaliaguine, *Experimental methods in chemical engineering: specific surface area and pore size distribution measurements—BET, BJH, and DFT.* The Canadian Journal of Chemical Engineering, 2019. **97**(11): p. 2781-2791.
[21] Vijayakumar, G., M. Dharmendirakumar, S. Renganathan, S. Sivanesan, G. Baskar, and K.P. Elango, *Removal of Congo red from aqueous solutions by perlite.* CLEAN–Soil, Air, Water, 2009. **37**(4-5): p. 355-364.
[22] Park, S.H., H.J. Cho, C. Ryu, and Y.-K. Park, *Removal of copper (II) in aqueous solution using pyrolytic biochars derived from red macroalga Porphyra tenera.* Journal of Industrial and Engineering Chemistry, 2016. **36**: p. 314-319.
[23] Chun, Y., G. Sheng, and C.T. Chiou, *Evaluation of current techniques for isolation of chars as natural adsorbents.* Environmental science & technology, 2004. **38**(15): p. 4227-4232.
[24] Hossain, M.A., H.H. Ngo, W.S. Guo, and T.V. Nguyen, *Palm oil fruit shells as biosorbent for copper removal from water and wastewater: experiments and sorption models.* Bioresource technology, 2012. **113**: p. 97-101.
[25] Kumar, M., A.K. Singh, and M. Sikandar, *Study of sorption and desorption of Cd (II) from aqueous solution using isolated green algae Chlorella vulgaris.* Applied Water Science, 2018. **8**(8): p. 225.
[26] Chen, W., H. Yu, Y. Liu, P. Chen, M. Zhang, and Y. Hai, *Individualization of cellulose nanofibers from wood using high-intensity ultrasonication combined with chemical pretreatments.* Carbohydrate Polymers, 2011. **83**(4): p. 1804-1811.
[27] Petrović, J.T., M.D. Stojanović, J.V. Milojković, M.S. Petrović, T.D. Šoštarić, M.D. Laušević, and M.L. Mihajlović, *Alkali modified hydrochar of grape pomace as a perspective adsorbent of Pb2+ from aqueous solution.* Journal of environmental management, 2016. **182**: p. 292-300.
[28] Elaigwu, S.E., V. Rocher, G. Kyriakou, and G.M. Greenway, *Removal of Pb2+ and Cd2+ from aqueous solution using chars from pyrolysis and microwave-assisted hydrothermal carbonization of Prosopis africana shell.* Journal of Industrial and Engineering Chemistry, 2014. **20**(5): p. 3467-3473.
[29] Mouni, L., D. Merabet, A. Bouzaza, and L. Belkhiri, *Adsorption of Pb (II) from aqueous solutions using activated carbon developed from Apricot stone.* Desalination, 2011. **276**(1-3): p. 148-153.
[30] Kula, I., M. Uğurlu, H. Karaoğlu, and A. Celik, *Adsorption of Cd (II) ions from aqueous solutions using activated carbon prepared from olive stone by ZnCl2 activation.* Bioresource technology, 2008. **99**(3): p. 492-501.
[31] Blázquez, G., F. Hernainz, M. Calero, and L.F. Ruiz-Nunez, *Removal of cadmium ions with olive stones: the effect of somes parameters.* Process Biochemistry, 2005. **40**(8): p. 2649-2654.
[32] Xu, H., D.C. Xu, and Y. Wang, *Natural indices for the chemical hardness/softness of metal cations and ligands.* ACS omega, 2017. **2**(10): p. 7185-7193.
[33] Zhou, N., H. Chen, Q. Feng, D. Yao, H. Chen, H. Wang, Z. Zhou, H. Li, Y. Tian, and X. Lu, *Effect of phosphoric acid on the surface properties and Pb (II) adsorption mechanisms of hydrochars prepared from fresh banana peels.* Journal of cleaner production, 2017. **165**: p. 221-230.
[34] Inyang, M., B. Gao, W. Ding, P. Pullammanappallil, A.R. Zimmerman, and X. Cao, *Enhanced lead sorption by biochar derived from anaerobically digested sugarcane bagasse.* Separation Science and Technology, 2011. **46**(12): p. 1950-1956.

[35] El-Ashtoukhy, E.S., N.K. Amin, and O. Abdelwahab, *Removal of lead (II) and copper (II) from aqueous solution using pomegranate peel as a new adsorbent.* Desalination, 2008. **223**(1-3): p. 162-173.

[36] Singh, E., A. Kumar, A. Khapre, P. Saikia, S.K. Shukla, and S. Kumar, *Efficient removal of arsenic using plastic waste char: Prevailing mechanism and sorption performance.* Journal of Water Process Engineering, 2020. **33**: p. 101095.

[37] Hu, G., Q. Tang, and D.-e. Jiang, *CoP for hydrogen evolution: implications from hydrogen adsorption.* Physical Chemistry Chemical Physics, 2016. **18**(34): p. 23864-23871.

[38] Rehman, S., A. Adil, A.J. Shaikh, J.A. Shah, M. Arshad, M.A. Ali, and M. Bilal, *Role of sorption energy and chemisorption in batch methylene blue and Cu 2+ adsorption by novel thuja cone carbon in binary component system: linear and nonlinear modeling.* Environmental Science and Pollution Research, 2018. **25**(31): p. 31579-31592.

[39] Yoo, G.Y., W.R. Lee, H. Jo, J. Park, J.H. Song, K.S. Lim, D. Moon, H. Jung, J. Lim, and S.S. Han, *Adsorption of Carbon Dioxide on Unsaturated Metal Sites in M2 (dobpdc) Frameworks with Exceptional Structural Stability and Relation between Lewis Acidity and Adsorption Enthalpy.* Chemistry–A European Journal, 2016. **22**(22): p. 7444-7451.

[40] Yang, G., S.A. Akhade, X. Chen, Y. Liu, M.S. Lee, V.A. Glezakou, R. Rousseau, and J.A. Lercher, *The Nature of Hydrogen Adsorption on Platinum in the Aqueous Phase.* Angewandte Chemie International Edition, 2019. **58**(11): p. 3527-3532.

[41] Sreedhar, I. and N.S. Reddy, *Heavy metal removal from industrial effluent using bio-sorbent blends.* SN Applied Sciences, 2019. **1**(9): p. 1021.

[42] Kalavathy, M.H., T. Karthikeyan, S. Rajgopal, and L.R. Miranda, *Kinetic and isotherm studies of Cu (II) adsorption onto H3PO4-activated rubber wood sawdust.* Journal of colloid and interface science, 2005. **292**(2): p. 354-362.

[43] Yao, Y., B. Gao, J. Fang, M. Zhang, H. Chen, Y. Zhou, A.E. Creamer, Y. Sun, and L. Yang, *Characterization and environmental applications of clay–biochar composites.* Chemical Engineering Journal, 2014. **242**: p. 136-143.

[44] Hu, X., Z. Ding, A.R. Zimmerman, S. Wang, and B. Gao, *Batch and column sorption of arsenic onto iron-impregnated biochar synthesized through hydrolysis.* Water Research, 2015. **68**: p. 206-216.

[45] Fernandez, M.E., B. Ledesma, S. Román, P.R. Bonelli, and A.L. Cukierman, *Development and characterization of activated hydrochars from orange peels as potential adsorbents for emerging organic contaminants.* Bioresource technology, 2015. **183**: p. 221-228.

[46] Wang, Z., G. Liu, H. Zheng, F. Li, H.H. Ngo, W. Guo, C. Liu, L. Chen, and B. Xing, *Investigating the mechanisms of biochar's removal of lead from solution.* Bioresource technology, 2015. **177**: p. 308-317.

[47] Dong, X., L.Q. Ma, and Y. Li, *Characteristics and mechanisms of hexavalent chromium removal by biochar from sugar beet tailing.* Journal of hazardous materials, 2011. **190**(1-3): p. 909-915.

[48] Abdel-Fattah, T.M., M.E. Mahmoud, S.B. Ahmed, M.D. Huff, J.W. Lee, and S. Kumar, *Biochar from woody biomass for removing metal contaminants and carbon sequestration.* Journal of Industrial and Engineering Chemistry, 2015. **22**: p. 103-109.

[49] Kim, W.-K., T. Shim, Y.-S. Kim, S. Hyun, C. Ryu, Y.-K. Park, and J. Jung, *Characterization of cadmium removal from aqueous solution by biochar produced from a giant Miscanthus at different pyrolytic temperatures.* Bioresource technology, 2013. **138**: p. 266-270.

[50] Özçimen, D. and A. Ersoy-Meriçboyu, *Characterization of biochar and bio-oil samples obtained from carbonization of various biomass materials.* Renewable Energy, 2010. **35**(6): p. 1319-1324.
[51] Jain, A., R. Balasubramanian, and M.P. Srinivasan, *Hydrothermal conversion of biomass waste to activated carbon with high porosity: A review.* Chemical Engineering Journal, 2016. **283**: p. 789-805.
[52] Titirici, M.M., A. Thomas, S.-H. Yu, J.-O. Müller, and M. Antonietti, *A direct synthesis of mesoporous carbons with bicontinuous pore morphology from crude plant material by hydrothermal carbonization.* Chemistry of Materials, 2007. **19**(17): p. 4205-4212.
[53] Roman, S., J.M.V. Nabais, B. Ledesma, J.F. González, C. Laginhas, and M.M. Titirici, *Production of low-cost adsorbents with tunable surface chemistry by conjunction of hydrothermal carbonization and activation processes.* Microporous and Mesoporous Materials, 2013. **165**: p. 127-133.
[54] Aydıncak, K., T.r. Yumak, A. Sınağ, and B. Esen, *Synthesis and characterization of carbonaceous materials from saccharides (glucose and lactose) and two waste biomasses by hydrothermal carbonization.* Industrial & Engineering Chemistry Research, 2012. **51**(26): p. 9145-9152.
[55] Huangfu, X., N. Xu, J. Yang, H. Yang, M. Zhang, Z. Ye, S. Wang, and J. Chen, *Transport and retention of hydrochar-diatomite nanoaggregates in water-saturated porous sand: Effect of montmorillonite and phosphate at different ionic strengths and solution pH.* Science of The Total Environment, 2020. **703**: p. 134487.
[56] Ghanim, B., J.G. Murnane, L. O'Donoghue, R. Courtney, J.T. Pembroke, and T.F. O'Dwyer, *Removal of vanadium from aqueous solution using a red mud modified saw dust biochar.* Journal of Water Process Engineering, 2020. **33**: p. 101076.
[57] Yoo, S., S.S. Kelley, D.C. Tilotta, and S. Park, *Structural characterization of loblolly pine derived biochar by X-ray diffraction and electron energy loss spectroscopy.* ACS Sustainable Chemistry & Engineering, 2018. **6**(2): p. 2621-2629.
[58] Fahmi, A.H., A.W. Samsuri, H. Jol, and D. Singh, *Bioavailability and leaching of Cd and Pb from contaminated soil amended with different sizes of biochar.* Royal Society Open Science, 2018. **5**(11): p. 181328.
[59] Sontakke, P., P. Jain, P. Yadav, V.K. Sharma, R.D. Sontakke, and V. Sontakke, *Efficacy of Indigenous, Unconventional Biosorbents in Defluoridation of Standard Water− An In Vitro Study.* Journal of Indian Association of Public Health Dentistry, 2017. **15**(1): p. 94.
[60] Clurman, A.M., O.M. Rodríguez-Narvaez, A. Jayarathne, G. De Silva, M.I. Ranasinghe, A. Goonetilleke, and E.R. Bandala, *Influence of surface hydrophobicity/hydrophilicity of biochar on the removal of emerging contaminants.* Chemical Engineering Journal, 2020. **402**: p. 126277.
[61] Hong, N., Q. Cheng, A. Goonetilleke, E.R. Bandala, and A. Liu, *Assessing the effect of surface hydrophobicity/hydrophilicity on pollutant leaching potential of biochar in water treatment.* Journal of Industrial and Engineering Chemistry, 2020.
[62] Khataee, A., B. Kayan, D. Kalderis, A. Karimi, S. Akay, and M. Konsolakis, *Ultrasound-assisted removal of Acid Red 17 using nanosized Fe3O4-loaded coffee waste hydrochar.* Ultrasonics sonochemistry, 2017. **35**: p. 72-80.
[63] Kambo, H.S. and A. Dutta, *A comparative review of biochar and hydrochar in terms of production, physico-chemical properties and applications.* Renewable and Sustainable Energy Reviews, 2015. **45**: p. 359-378.
[64] Ahsan, S., M.A. Rahman, S. Kaneco, H. Katsumata, T. Suzuki, and K. Ohta, *Effect of temperature on wastewater treatment with natural and waste materials.* Clean Technologies and Environmental Policy, 2005. **7**(3): p. 198-202.

[65] Mahmoud, M.A. and M.M. El-Halwany, *Adsorption of cadmium onto orange peels: isotherms, kinetics, and thermodynamics.* J Chromatogr SepTech, 2014. **5**(238): p. 2.
[66] Protopopoff, E. and P. Marcus, *Potential-pH diagrams for Pb adsorption on Cu and Ni surfaces at 25 C and 300 C.* Journal of The Electrochemical Society, 2013. **160**(3): p. C106.
[67] Çatlıoğlu, F.N., S. Akay, B. Gözmen, E. Turunc, I. Anastopoulos, B. Kayan, and D. Kalderis, *Fe-modified hydrochar from orange peel as adsorbent of food colorant Brilliant Black: process optimization and kinetic studies.* International Journal of Environmental Science and Technology, 2020. **17**(4): p. 1975-1990.
[68] Rehman, M., L. Liu, Q. Wang, M.H. Saleem, S. Bashir, S. Ullah, and D. Peng, *Copper environmental toxicology, recent advances, and future outlook: A review.* Environmental Science and Pollution Research, 2019: p. 1-14.
[69] Omar, S., M.S. Muhamad, L. Te Chuan, T. Hadibarata, and Z.C. Teh, *A review on lead sources, occurrences, health effects, and treatment using hydroxyapatite (HAp) adsorbent made from fish waste.* Water, Air, & Soil Pollution, 2019. **230**(12): p. 275.
[70] https://www.epa.gov/eg/industrial-effluent-guidelines
[71] World Health Organization, Guidelines for Drinking-Water Quality: Fourth Edition Incorporating the First Addendum, Geneva, 2014: p.541.

Supplementary information

Removal of heavy metals from water using engineered hydrochar: Kinetics and mechanistic approach

Kannan Nadarajah[1,2,3], Erick R. Bandala[4], Zhanying Zhang[3], Sagadevan Mundree[3], Ashantha Goonetilleke[1,3*]

[1] School of Civil and Environmental Engineering, Queensland University of Technology, GPO Box 2344, Brisbane 4001, Queensland, Australia

[2]Department of Agricultural Engineering, Faculty of Agriculture, University of Jaffna, Sri Lanka

[3] Center for Agriculture and Bioeconomy, Institute for Future Environments, Queensland University of Technology, 2 George St, Brisbane, Queensland 4000, Australia

[4]Division of Hydrologic Sciences, Desert Research Institute, 755 E. Flamingo Road, Las Vegas, NV89119-7363, USA

[*] Corresponding author

E-mail: a.goonetilleke@qut.edu.au.

Postal address: School of Civil and Environmental Engineering, Queensland University of Technology, GPO Box 2344, Brisbane 4001, Queensland, Australia

1.1 S: Isotherm, Kinetic, rate limiting factor and thermodynamic analyses of engineered hydrochar for Pb^{2+} and Cu^{2+} removal

For isotherm analysis, Langmuir, Freundlich and Temkin models were used.

Langmuir isotherm model is expressed as shown in equation 1:

$$q_e = \frac{q_m k_L c_e}{1+k_L c_e} \quad (1)$$

The equation 1 was converted into linearised form for better interpretation of data as shown in equation 2.

$$\frac{C_e}{q_e} = \frac{1}{q_m k_L} + \frac{C_e}{q_m} \quad (2)$$

C_e and q_e are equilibrium metal concentrations in solution (mg/L) and equilibrium sorption capacity (mg/g), respectively. q_m (mg/g) and k_L (L/mg) are Langmuir constants related to maximum sorption capacity and energy of sorption, respectively.

Freundlich isotherm model is expressed as shown in equation 3:

$$q_e = k_F C_e^{\frac{1}{n}} \quad (3)$$

The equation 4 represents the linear form of the Freundlich isotherm.

$$\log q_e = \log k_F + {}^1/_n \log C_e \quad (4)$$

Where k_F is Freundlich constant (mg/g) and n is the Freundlich exponent. Values of k_F and n were used to indicate sorption capacity and intensity of reaction, respectively. Moreover, nature of interaction was predicted using n values.

Temkin isotherm is expressed as shown in equation 5:

$$q_e = B_T \ln A_T + B_T \ln C_e \quad (5)$$

Where qe is the amount of sorbate at equilibrium (mg/g) and C_e is the concentration of sorbate in solution at equilibrium (mg/L). B_T is a constant related to heat of sorption and B_T=RT/b, where b is the Temkin constant J/mol, T is the absolute temperature (K), R is the gas constant (8.314 J/mol.K) and A_T is the Temkin isotherm constant (L/g). From the plot of qe Vs ln C_e, B_T and A_T were calculated from the slope and intercept, respectively.

For kinetics analysis, Pseudo first order and Pseudo second order models were used.

The Pseudo first order model is expressed as shown in equation 6:

$$\frac{dq_t}{dt} = K_1 (q_e - q_t) \quad (6)$$

Integrating equation 6 yielded linearised form as shown in equation 7.

$$\ln(q_e - q_t) = \ln q_e - k_1 t \quad (7)$$

Therefore, the slope of the graph of ln (q_e - q_t) Vs t was used to determine the pollutant binding rate.

Pseudo Second order model is expressed as shown in equation 8:

$$\frac{dq}{dt} = k_2 (q_e - q_t)^2 \quad (8)$$

By integrating equation 8, the linearised form of the Pseudo second order equation was obtained as shown in equation 9.

$$\frac{t}{q_t} = \frac{1}{k_2 q_e^2} + \frac{1}{q_e} t \quad (9)$$

Where k_1 is the pseudo-first order rate constant (L/min) and k_2 is the pseudo-second order rate constant (g/(mg.min)). The initial adsorption rate, h (mg/ (g.min)) at t = 0 is defined as $h = k_2^2 qe^2$. Equilibrium sorption capacity was found from the graph of t/q_t Vs t.

Rate limiting factor analysis

The Weber-Morris model was used to interpret diffusive scenarios because of its practical viability. The Weber - Morris model is expressed as shown in equation 10:

$$Q_t = K_{wm}\sqrt{t} + I \quad (10)$$

Where K_{wm} is the Weber - Morris constant related to intraparticle diffusion rate and I is the y - intercept related to the boundary layer thickness. Interpretation of sorption data using linear regression techniques yields K_{wm}.

Thermodynamics

Thermodynamic parameters such as the changes in the standard free energy (ΔG_0), the enthalpy (ΔH_0) and the entropy (ΔS_0) associated with the adsorption process were determined using the rate equation (equation 10) and the Van't Hoff equation (equation 14). Moreover, parameters such as enthalpy change (ΔH_0), entropy change (ΔS_0) and free energy change (ΔG_0) were used to predict the flexibility and spontaneity of the sorption process. The ΔG_0 and K_D, were evaluated by equations 11 and 12, respectively.

$$\Delta G^o = -RT\ln K_D \quad (11)$$

Where R is the universal gas constant, T is the absolute temperature and K_D is the distribution co-efficient

$$K_D = \frac{(C_o - C_e)}{(\frac{m_s}{v})C_e} \quad (12)$$

Where, m_s and v are mass of sorbent and volume of solution, respectively.

In addition to the above version, ΔG_0 was defined in terms of ΔH_0 and ΔS_0 as shown in equation 13:

$$\Delta G^o = \Delta H^o - T\Delta S^o \quad (13)$$

ΔH_0 and ΔS_0 were calculated from the slope and intercept of log K_D Vs 1/T plot respectively, as show in equation 14.

$$\log K_D = \frac{\Delta S^o}{2.303R} - \frac{\Delta H^o}{2.303RT} \quad (14)$$

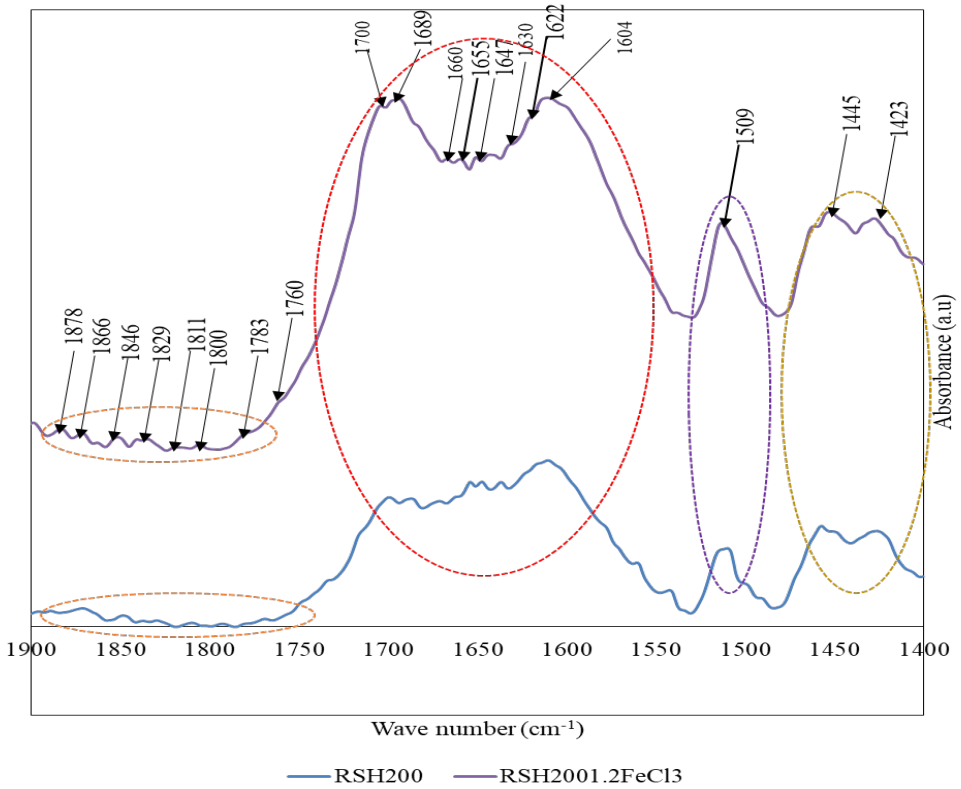

Fig. S1. FTIR active region of catalyzed and non-catalyzed hydrochars

Fig. S2. Kinetic models for Pb^{2+} adsorption to customised hydrochar: (a) Pseudo first order; (b) Pseudo second order

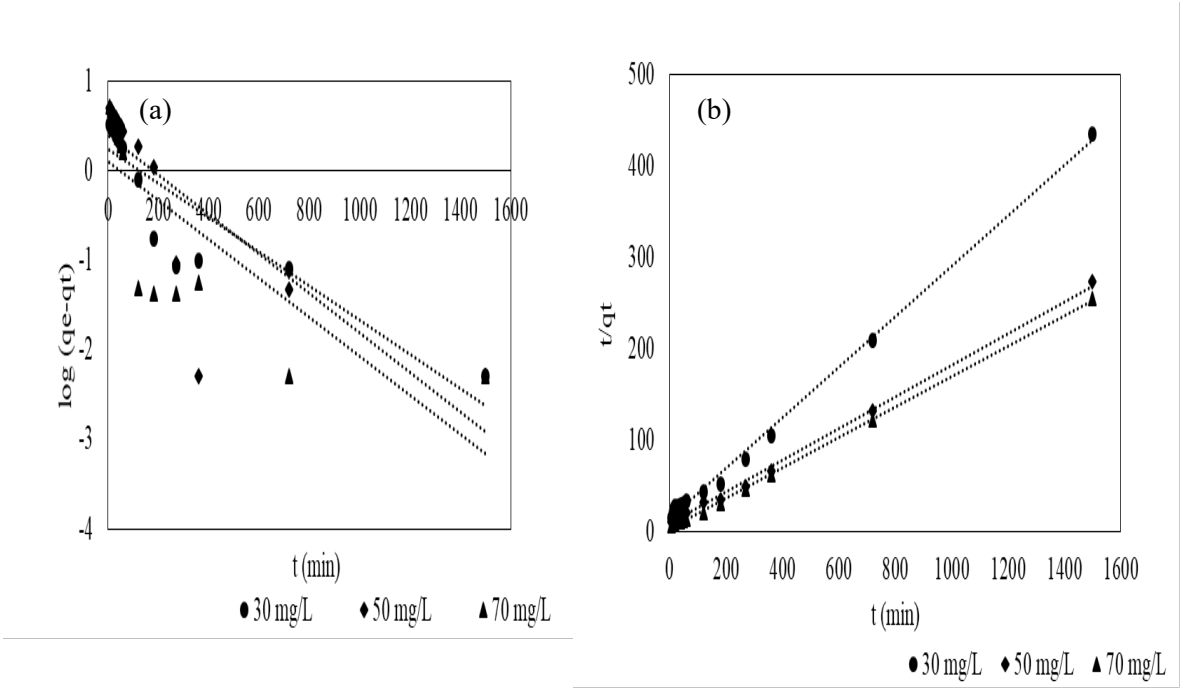

Fig. S2. Kinetic models for Pb^{2+} adsorption to customised hydrochar: (a) Pseudo first order; (b) Pseudo second order

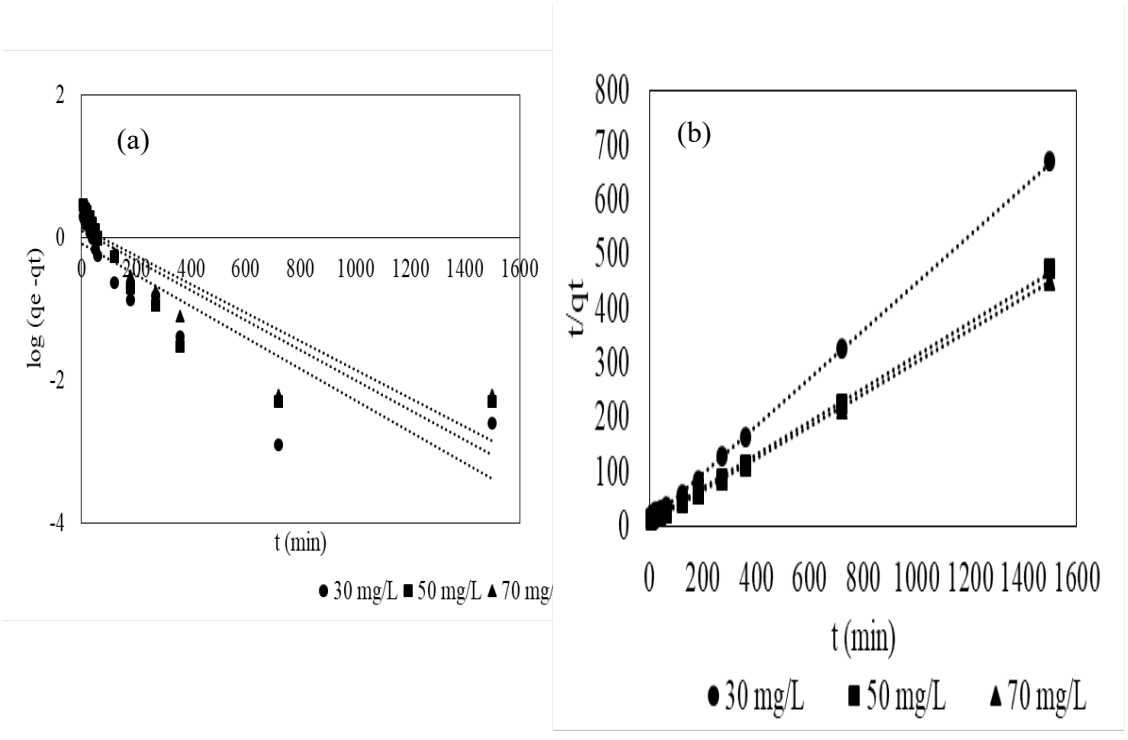

Fig. S3. Kinetic models for Cu^{2+} adsorption to customised hydrochar: (a) Pseudo first order; (b) Pseudo second order.

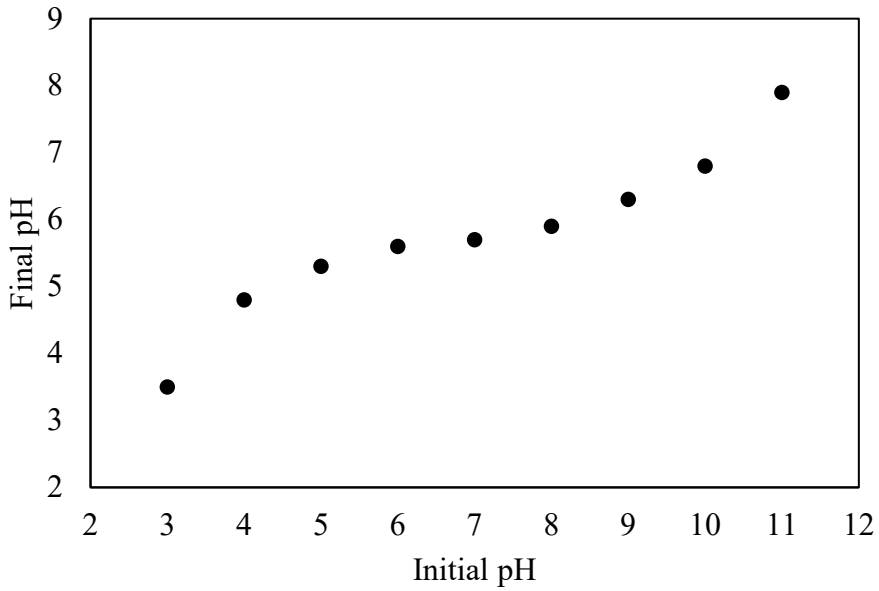

Fig. S4. Point zero charge (pzc) of engineered hydrochar

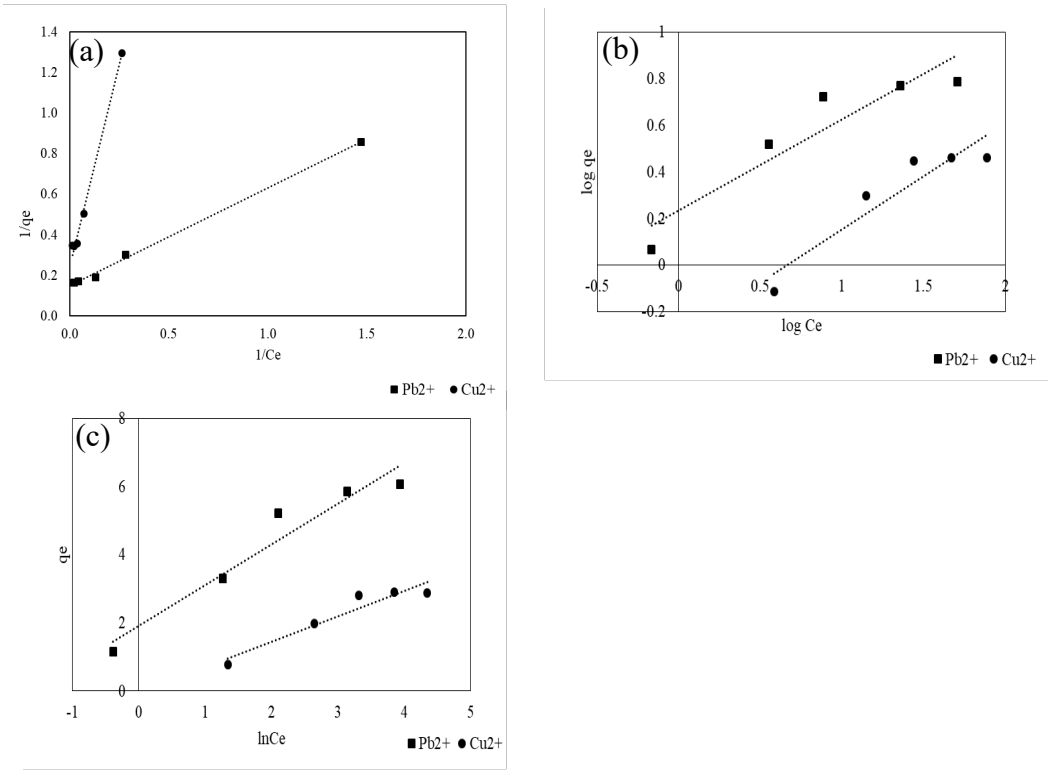

Fig. S5: Isotherm models for Pb^{2+} and Cu^{2+} adsorption to customised hydrochar; (a) Langmuir; (b) Freundlich; (c) Temkin

Note: Ce - equilibrium concentration (mg/L); qe - equilibrium amount of Pb^{2+}/Cu^{2+} ions adsorbed onto the hydrochar (mg/g).

Table S1: Detailed analysis of FTIR band peaks of engineered hydrochar

Band peak	Causes of peaks	Nature of peak	Hydrophobicity/ Hydrophilicity
3301	**Hydroxyl (-OH stretching of H bonded and free) (acidic -OH)**	**Strong**	**Hydrophilic**
2823 and 2890	Alkane (C-H stretching)	Strong	Hydrophobic
2138 and 1957	Silane (Stretching)	Strong	Hydrophobic
1669	**Carbonyl (-CO stretching)**	**Strong**	**Hydrophilic**
1586	**Amine (-NH bending)**	**Medium**	**Hydrophilic**
1338, 1403 and 1469	**Alkane (C-H bending)**	**Strong**	**Hydrophobic**
1338	CN stretching	medium	Hydrophilic
1156 and 1204	**Carbonyl (ether)(-CO stretching) and alcoholic -OH stretching**	**Strong**	**Hydrophilic**
1063	**Carbonyl -CO stretching**	**Strong**	**Hydrophilic**
781	-SOR stretching	Strong	Hydrophilic